Evolution and emplacement of high fluorine rhyolites in the Mesoproterozoic Gawler silicic large igneous province, South Australia

Authors: Agangi, Andrea*, Kamenetsky, Vadim S., McPhie, Jocelyn

ARC Centre of Excellence in Ore Deposits and School of Earth Sciences, University of Tasmania, Private bag 79, Hobart, Tasmania 7001, Australia

*Corresponding author. Present address Paleoproterozoic Mineralisation Group, Department of Geology, University of Johannesburg, Auckland Park 2006, South Africa. Tel.: +27 (0)11 559 4701; fax: +27 (0)11 559 4702; email: aagangi@uj.ac.za (A. Agangi)

Abstract

The Gawler Range Volcanics (GRV) and the Hiltaba Suite (HS) of South Australia form a silicic-dominated large igneous province (the Gawler SLIP) emplaced in an intracontinental setting during the Mesoproterozoic. Emplacement of the GRV lasted for a short period of time (~2 Ma), and can be separated into two main phases. The first phase (lower GRV) is composed of thick (≤3 km) sequences erupted from distinct centres, and includes small to moderate volume (up to >150 km^3) felsic lavas, ignimbrites, and minor mafic and intermediate lavas. The upper GRV include extensive felsic lavas that are up to >1000 of km^3 in volume and >200 km across. Using well preserved, quartz-hosted melt inclusions, we investigated the composition of the lower GRV, including major, trace, and volatile elements. The results indicate high concentrations of K_2O (≤7 – 8 wt.%), rare earth and high field strength elements, and low concentrations of Ca, Mg, Ni, Cr, Sr and Ba in comparison with felsic continental crust. Overall, melt inclusion compositions match whole-rock geochemical characteristics. We demonstrate that the GRV magma was F-rich (≤1.3 wt.%), and had high temperature for a silicic magma. High F concentrations and high temperature would have resulted in lower-than-usual polymerisation of the melt and relatively low viscosity. These characteristics help explain how very voluminous felsic magma was erupted effusively and emplaced as lavas. Other intracontinental SLIP contain extensive felsic lavas and ignimbrites which appear to share similar geochemical characteristics. We also show that selective alteration caused depletion of whole-rock compositions in some trace elements, namely Pb, U, and Sn.

1. Introduction

Large igneous provinces (LIP) are vast amounts of magma erupted onto the Earth's surface or injected into the crust in pulses of relatively short duration and at high emplacement rates (Bryan and Ernst, 2008; Coffin and Eldholm, 1994; Ernst et al., 2005). Emplacement of LIP has occurred throughout geological time in both intraplate and plate margin settings, and is distinct from seafloor spreading and subduction-related magmatism

(Mahoney and Coffin, 1997; Hamilton and Buchan, 2010). Most LIP are mainly mafic, and include flood basalts, giant dolerite dyke swarms, and layered intrusions (Head and Coffin, 1997), but in some, felsic units can be conspicuous (e.g. felsic rocks associated with the Paraná-Etendeka continental flood basalt province, Ewart et al., 1998a; Milner et al., 1992; Peate, 1997).

Silicic-dominated large igneous provinces (SLIP) of similar dimensions to the mafic provinces (≥10^5 km^3) are less common. Known examples are mostly Phanerozoic, and include the Sierra Madre Occidental of Mexico (Bryan et al., 2008; Cameron et al., 1980; Ferrari et al., 2002), the Trans-Pecos volcanic field of the USA (Henry et al., 1988; Parker and White, 2008), the Chon-Aike Province of South America and Antarctica (Pankhurst et al., 1998; 2000; Pankhurst and Rapela, 1995; Riley et al., 2001), the Snake River Plain of the western USA, Branney et al., 2008), the Whitsunday Volcanic Province of eastern Australia (Bryan, 2002; 2007; Bryan et al., 2000), and the Gawler Range Volcanics of South Australia (McPhie et al., 2008) (Table 1). Some of these provinces include extensive felsic lavas the dimensions of which are comparable with flood basalts (e.g. Star Mountain Rhyolite, Trans-Pecos, Henry et al., 1988; Yardea Dacite, Gawler Range Volcanics, Allen and McPhie, 2002; Allen et al., 2003; Keweenawan Midcontinent Rift plateau volcanic units, Green and Fitz, 1993), whereas others are dominated by extensive ignimbrites (e.g. Bryan et al., 2000). Some key questions for SLIP research are related to the eruption and emplacement mechanisms: how are these large volumes of felsic magma emplaced over short time spans? Are SLIP erupted explosively or effusively? If extensive felsic units are emplaced effusively (flood rhyolites), how can felsic lava flow for very long distances?

In this contribution, we describe the volcanic facies of the 1.6 Ga Gawler Range Volcanics (GRV)-Hiltaba Suite (HS) silicic-dominated LIP (the Gawler SLIP) of South Australia to evaluate its emplacement mechanisms (explosive versus effusive). We also present analyses of well preserved quartz-hosted melt inclusions to reconstruct the composition of source magmas. Melt inclusions are droplets of silicate melt trapped within crystals growing in a magma. If preserved, they represent samples of pristine silicate liquid (melt) unaffected by modifications occurring as the magma approaches the Earth's surface. Melt inclusions can be studied as a powerful tool to assess the pre-emplacement volatile content of a magma (Métrich and Clocchiatti, 1989; Lowenstern and Mahood, 1991; Lowenstern, 1995) and to reconstruct the magma composition in altered or mineralised rocks (Chabiron et al., 2001). Melt inclusions also give the opportunity to study the influence of crystal fractionation on melt evolution, without the effects of crystal accumulation encountered when using whole-rock analyses.

2. The Gawler SLIP

The GRV and co-magmatic HS granite represent a silicic-dominated LIP (the Gawler SLIP) with a preserved (minimum) volume of ~100 000 km^3, of which ~25 000 km^3 are represented by the volcanic sequence (Blissett et al., 1993; McPhie et al., 2008; Fig. 1). To the east, the province is partially concealed underneath younger Proterozoic and Phanerozoic sediments of the Stuart Shelf (Blissett et al., 1993). The province includes several voluminous (tens of km^3 to >1000 km^3) and extensive (tens to >200 km across) felsic lavas and ignimbrites (Allen et al., 2008; Blissett et al., 1993) and minor mafic to intermediate units. The Gawler SLIP was emplaced in a subaerial intracontinental setting, and lies on Archean and Paleoproterozoic units of the Gawler Craton (Allen and McPhie, 2002; Allen et al., 2008; Betts and Giles, 2006; Blissett et al., 1993; Creaser, 1995). U-Pb zircon dating of the volcanic units has yielded a narrow age range of 1591-1592 Ma (Creaser, 1995; Creaser and Cooper, 1993; Fanning et al., 1988), whereas ages of the HS granites range from 1583 ±7 to 1598 ±2 Ma (Flint, 1993).

Emplacement of the Gawler SLIP is temporally related with high temperature low pressure metamorphism in the region (the Hiltaba event; Betts and Giles, 2006; Betts et al., 2002), and coeval with the 1.6-1.3 Ga intraplate magmatic event that occurred throughout Laurentia and Baltica (Anderson and Morrison, 2005). It has been hypothesised that the GRV were emplaced as part of a hotspot-related igneous activity affecting the central part of Australia (Betts et al., 2009). The Gawler SLIP is associated with a major metallogenic event that affected most of the Gawler Craton (Budd and Fraser, 2004; Fraser et al., 2007; Skirrow, 2002; Skirrow et al., 2007). The Au-U Olympic Dam deposit was formed during this event.

The GRV have been subdivided into lower and upper sequences based on the discordance between small to moderate volume, gently to moderately dipping older units and extensive, nearly flat-lying younger units (Blissett et al., 1993). The lower GRV consist of thick (up to 3 km) successions, erupted from several discrete volcanic centres. Evenly porphyritic dacite and rhyolite are interbedded with ignimbrites and volumetrically minor mafic lavas (basalt and basaltic andesite). The Chitanilga Volcanic Complex at Kokatha (Blissett, 1975; 1977b; Branch, 1978; Stewart, 1994) and the Glyde Hill Volcanic Complex at Lake Everard (Blissett, 1975; 1977a; 1977b; Ferris, 2003; Giles, 1977) are the two best exposed parts of the lower GRV (Fig. 1b, c) and are the subject of this study. The upper GRV are composed of at least three large-volume (>1000 km^3), extensive (≤200 km), evenly porphyritic and compositionally homogeneous felsic (dacite and rhyolite) massive lavas (Allen and McPhie, 2002; Allen et al., 2008; Creaser and White, 1991; McPhie et al., 2008). Units in the upper GRV are up to 300 m thick, and as a whole, crop out for 12 000 km^2. Mineral assemblages in the upper GRV are essentially anhydrous and include phenocrysts of plagioclase (oligoclase-andesine), K-feldspar, orthopyroxene (pigeonite Mg# 24-43, augite

Mg#30-53), Fe-Ti oxide, ±quartz in a quartz-feldspar groundmass (Creaser and White, 1991; Stewart, 1994).

The GRV sequence is cross-cut by numerous porphyritic rhyolite, and less abundant andesite, dykes (Blissett et al., 1993). The Moonamby Dyke Suite (Giles, 1977) includes rhyolite porphyritic dykes that intruded the lower GRV at Lake Everard. The HS granite includes large batholiths and smaller intrusions of granite and minor quartz monzodiorite and quartz monzonite (Flint, 1993). Typical of much of the HS is medium-grained, locally porphyritic pink granite composed of quartz, alkali-feldspar, plagioclase, minor interstitial biotite, apatite and fluorite. HS granite intruded the GRV at various localities with sharp contacts and no major of metamorphic overprint in the host volcanic rocks (Blissett, 1985; Giles, 1988). The GRV are essentially undeformed and unmetamorphosed and primary textures are well preserved, in spite of the moderate alteration of feldspar.

3. Analytical methods

Whole-rock chemical analysis

Samples were crushed in a WC mill for X-ray fluorescence (XRF) and inductively coupled plasma mass spectrometry (ICP-MS) whole-rock analysis at the University of Tasmania. Major and some trace elements (V, Cr, Ni, Cu, Zn, Rb, Sr, Y, Zr, Nb, Ba, and La) were measured by XRF, trace elements were analysed by ICP-MS. Samples were digested in HF/H_2SO_4 with the PicoTrace high pressure digestion equipment and analysed with an Agilent 4500 ICP-MS. XRF analyses were made with a Philips PW1480 X-ray Fluorescence Spectrometer. Detection limits for trace elements in ICP-MS are ≤0.01 ppm (REE) and ≤0.5 ppm for other elements, except As (5 ppm). Comparison of XRF and ICP-MS trace element data indicates a good correlation between the XRF and ICP-MS trace element data, the difference being <20% relative.

Melt inclusion sample preparation and major-trace element analysis

Samples selected for melt inclusion study were crushed in a steel mortar and sieved. Batches of quartz grains (fractions 0.4-1 mm) were heated in a furnace at 1 atm pressure to temperatures between 800° and 1050°C at 50°C intervals for 24 hours. Heating experiments were only carried out once for each batch of grains. During heating sessions, quartz grains were wrapped in platinum foil to avoid contamination (Kamenetsky and Danyushevsky, 2005). After heating, the grains were water-quenched and mounted in epoxy resin for inspection. Grains selected for analysis were extracted and individually mounted in single-grain mounts moulded in aluminium or brass tubes. Melt inclusions were then exposed and polished for analysis.

Electron probe microanalyses (EPMA) of a total of 65 melt inclusions were carried out with a 5-spectrometer SX-100 Cameca microprobe. Operating conditions of 15 kV acceleration potential difference, 10 nA beam current, counting time between 10 and 30 s, and 5 µm spot size were used. Since heat-induced diffusion of elements under the electron beam can result in underestimation of some components, the most volatile elements (K, Na, F) were analysed first and the signal intensity was monitored during analyses. No significant loss in signal intensity was observed. As a reference material, USGS glass BSR-2G was chosen. Major element analyses on the standard glass show good agreement (<10% relative) with data published by GeoRem and USGS. Diffusion of volatile elements (Chabiron et al., 2001) and metals (Kamenetsky and Danyushevsky, 2005) can occur during heating experiments, so both heated and unheated inclusions were analysed for comparison.

Eighteen melt inclusions were also analysed for trace elements on a Resonetics M50 excimer laser coupled with an Agilent 7500cs ICP-MS. Energy was 2 J/cm^2 at 5 Hz repetition frequency. Spot size (20 - 60 µm) was comparable or slightly larger than melt inclusion size, but the relatively low laser energy allowed ablation of only the glass inclusions and not the host quartz. Ablation time was 60 s per inclusion. Glass NIST 612 was used as a standard and glass BCR-2G was used as a secondary standard. Aluminium, measured by EPMA, was used as the internal standard. The signal was stable to steadily decreasing and lacked peaks, indicating that the glass was homogeneous. Comparison with published standard compositions (Georem) indicates an error within 20% relative.

4. The Glyde Hill and Chitanilga Volcanic Complexes

The Glyde Hill Volcanic Complex

The Glyde Hill Volcanic Complex is dominated by felsic units (>90 %); minor andesite and very minor basalt are present (Fig. 2). Felsic to silica-rich intermediate units (SiO_2 >60 wt.%) range in extent from ~10 km to >80 km across and are up to a few hundreds of metres thick. The volumes, estimated on the basis of the outcrop extent, range between ≤1 km^3 (Whyeela Dacite, Andesite I) and ~170 km^3 (Yantea Rhyolite-dacite). Aspect ratio (ratio of diameter of circle with equivalent area and mean thickness) is up to ~1:250 (Table 2).

All the felsic lava units are evenly porphyritic; phenocrysts of albite, K-feldspar and ±quartz (<1 to >10 vol.%) are set in a microcrystalline, probably formerly glassy groundmass (Fig. 3a, b, Table 3). Phenocrysts are anhedral to euhedral, and largely unbroken. The most common accessory minerals are zircon, F-apatite, and Fe-Ti oxide. Most of the felsic lavas show cm-scale flow bands and flow lineations, and locally sheet parting. In some units (Wheepool Rhyolite, Yantea Rhyolite-dacite), flow bands are planar to folded in open to tight folds at the metre-scale. The Baldry Rhyolite shows evidence of intense flow deformation that produced non-cylindrical folds (sheath folds) in the interior of the unit, and a cm-thick vesicular carapace. Sheath folds are characterised by folded axis and sub-parallelism between fold axis and flow lineation (Fig 3c). In sections perpendicular to the direction of flow, flow bands describe round or elongate concentric structures, representing intersections of culminations of folded axes (Fig. 3d). Spherulitic texture and lithophysae are locally present. Several units (Childera Rhyolite, Mangaroongah Dacite, Wheepool Rhyolite, Baldry Rhyolite, and Yantea Rhyolite-dacite) contain clast-supported monomictic breccia domains composed of either angular or lobate, porphyritic and amygdaloidal clasts set in porphyritic, flow banded or vesicular/amygdaloidal matrix (Fig. 3e, f). These zones, which are up to a few m thick and crop out for up to tens of m, are interpreted as autobreccia, and developed during viscous flow. The base of the Yantea Rhyolite-dacite is locally peperitic where the dacite has mingled with a fine grained deposit. The lobed outcrop distribution of the Yantea Rhyolite-dacite east of Lake Everard (Fig. 1c) suggests that the flow infilled an irregular topography.

Pyroclastic facies are very minor in the Glyde Hill Volcanic Complex, and include vitric ash tuff (Fig. 3g), composed of crystals and crystal fragments (<20 vol.%, feldspar and quartz), and minor lithic fragments (<5 vol.%) set in a non-welded bubblewall-shard matrix (Table 3). Layers of breccia are also intercalated in the Mangaroongah and Childera Dacites. These breccias include cm-scale angular pumice or feldspar-phyric clasts in mm-sized matrix, and are interpreted as the products of minor explosive episodes that accompanied the main effusive activity.

Intermediate (andesite sensu lato: andesite, trachyandesite and trachyte, SiO_2 = 58 – 63 wt.%) and mafic-intermediate units (Nuckulla Basalt, basalt and basaltic (trachy)andesite, SiO_2 ≤52 wt.%) occur in limited areas, <10 km across, and are volumetrically minor. These units are mostly massive and evenly porphyritic with sparse phenocrysts of clinopyroxene ±plagioclase in a microcrystalline groundmass of plagioclase, amphibole-altered clinopyroxene, and magnetite.

The Moonamby Dyke Suite includes several quartz-feldspar-phyric rhyolite dykes (Fig. 3h) that cross-cut the Glyde Hill Volcanic Complex. These dykes are up to 100 m wide and crop out for up to 10-20 km, trending northwest to north-northeast.

Felsic igneous enclaves, centimetres to meters in size and composed of mm-scale anhedral crystals of quartz and K-feldspar in a microcrystalline quartzo-feldspathic groundmass are present in different volcanic units (Fig. 1b, c). Felsic igneous enclaves have gradational margins with the host volcanic rock (Fig. 4a), and are associated with the occurrence of anhedral quartz and K-feldspar grains scattered in the host rocks. These enclaves contain crystals of anhedral K-feldspar and amoeboid quartz (approximately 50 % vol.), separated by a microcrystalline quartz +K-feldspar +albite groundmass (Fig. 4b). Feldspar crystals are in many cases surrounded by a granophyric rim, up to 0.5 mm-thick, formed by an intergrowth of elongate K-feldspar and quartz (Fig. 4c). These intergrowths make up 10 – 20 vol.% of the groundmass and only occur around K-feldspar. Quartz can be found as single rounded to amoeboid crystals, <0.5 mm across (partially resorbed magmatic quartz), or in round to lobed aggregates, 0.5 to 1 mm in size, associated with epidote and minor, fluorite, chlorite and titanite (“late” quartz, Fig. 4d). Accessory minerals include zircon, magnetite, fluorite, Ti-oxide, and epidote. These enclaves are interpreted as partially re-melted granite or crystal mush blocks. Similar enclaves have been described by Garner and McPhie (1999) in the Yardea Dacite of the upper GRV. Part of these enclaves have similar textures and mineral assemblage to the ones described here, but larger size (up to 50 m), and have been interpreted as partially melted HS granite (Garner and McPhie, 1999).

The Chitanilga Volcanic Complex

The Chitanilga Volcanic Complex includes a thick sequence (~3 km) of alternating lavas and pyroclastic units (Fig. 2) dipping to the southeast at a moderate angle (≤30°). The base of the sequence is concealed under Quaternary deposits. The lower part (~1 km) of the exposed sequence is composed of m-thick mafic to intermediate lava units (vesicular/amygdaloidal basalt and basaltic andesite), and interlayered felsic ignimbrite and other volcaniclastic units, each up to several tens of metres thick. These lavas are sparsely porphyritic and include phenocrysts of magnetite- and amphibole-altered ferromagnesian minerals (olivine?), and microphenocrysts of plagioclase in a microcrystalline plagioclase and magnetite groundmass.

The upper part of the sequence is dominated by felsic lavas and ignimbrites, and also includes minor intermediate lava. These intermediate to felsic lava units are up to several hundreds of metres thick and extend for up to 20 km. Aspect ratio is up to ~1:30 (Table 2). The volumes, estimated on the basis of the outcrop extent, range from <<1 km^3 (Andesite) to >20 km^3 (Chandabooka Dacite). Felsic lavas are all evenly porphyritic and include 5 – 10 vol.% phenocrysts of alkali feldspar ±minor quartz (Table 3). Phenocrysts are mostly anhedral (feldspar is sieve-textured and quartz is round or embayed), but unbroken. Millimetre-scale, anhedral (round or amoeboid) quartz and feldspar are locally present, and are associated with felsic massive or banded igneous enclaves (Rhyolite-dacite Mi5). The groundmass is microcrystalline and composed of K-feldspar, albite and quartz. Bedding-parallel fiamme are locally present at the base of one unit (Rhyolite-dacite Mi2), and interpreted to be welded autobreccia. The 600-metre thick Rhyolite-dacite (Mi2) conformably overlies the mafic lavas and shows gently to steeply dipping flow folded flow bands, flow lineation and, locally, aligned amygdales. The Chandabooka Dacite lies at the top of the succession and has been correlated with the Yardea Dacite of the upper GRV (Blissett, 1985). It is locally flow banded at the mm-scale and contains phenocrysts of plagioclase (albite) in a microcrystalline quartzo-feldspathic groundmass. The unit is separated from the rest of the underlying sequence by a thick and laterally continuous, massive, clast-supported breccia zone.

The pyroclastic units are up to 400 m thick and extend for up to a few tens of km. These units are massive to bedded/foliated (fiamme bearing or compositionally layered at the mm- to cm-scale; Fig. 5a). They contain a variable amount of feldspar and quartz crystals or crystal fragments (≤few mm, average 20 vol.%) set in a very fine-grained eutaxitic or banded matrix. Devitrified glass shards and flattened pumice fragments (fiamme) are preserved in moderately welded ignimbrites and better preserved parts of rheomorphic ignimbrites. In more welded domains, where glass shards are not present, evidence of fragmental origin is provided by occurrence of angular crystal fragments (Fig. 5b). Lithic fragments are scarce to absent.

Some small-volume pyroclastic units are interbedded with the basalt at the base of the Chitanilga Volcanic Complex, indicating coeval felsic and mafic magmatic activity, although probably from different sources. These pyroclastic units are up to 100 m thick and laterally continuous and include non- to relatively welded, fiamme-bearing or cm-scale layered ignimbrites. The matrix is fine grained, eutaxitic and vitriclastic to microcrystalline. The Lake Gairdner Rhyolite is a 400-m-thick multiple-flow unit ignimbrite with a massive to eutaxitic texture, defined by fiamme (flattened and aligned pumice clasts) or by flattening of rare lithic components in the matrix (Fig. 5a). K-feldspar, albite and quartz crystal and crystal fragments are set in a variably compacted bubble-wall shard matrix (Fig. 5a, b).

The 200-m-thick Rhyolite-dacite (Mi5) overlies the Andesite and, locally, the Lake Gairdner Rhyolite east of Kokatha (Fig. 1c). The base of the unit shows a cm-scale, planar discontinuous bedding/lamination, conformable with the underlying unit. The middle and top parts are bedded and flow-folded (Fig. 5c-f). The mm- to cm-scale beds are defined by alternating crystal-rich, internally massive layers, and crystal-poor, internally finely banded and flow-deformed layers. The beds are variably flow-deformed in open to tight, isoclinal, and sheath folds (Fig. 5c-e). Ptygmatic folds are also present, and indicate vertical shortening. The orientation of axial planes of asymmetric folds, their vergence, and flow lineation (Fig. 5f) indicate east-northeast-directed viscous flow.

5. Melt inclusion description and heating experiments

Three units, the Wheepool Rhyolite, the Waurea Pyroclastics, and the Moonamby Dyke Suite, contain well preserved quartz phenocryst-hosted melt inclusions.

The Wheepool Rhyolite (samples GH06, 23, 24c, 59) comprises massive or flow-banded porphyritic lavas. Phenocrysts (~10 vol.%) are euhedral to subhedral plagioclase (albite) and K-feldspar (perthite), and minor (≤1 vol.%) subhedral to anhedral quartz, mostly ≤1 mm in diameter. The microcrystalline to micropoikilitic groundmass (<10 to 50 μm) is mainly composed of quartz, K-feldspar and plagioclase (albite) (Fig. 3a). The Waurea Pyroclastics (samples GH13, 95) include several different pyroclastic facies that vary in grain size, composition and texture. One of the facies is violet to pale grey, relatively poorly sorted crystal tuff (Fig. 3g), in which quartz is a main component (5-10 vol.%), other than K-feldspar, minor plagioclase (albite), and lithic fragments (<5 vol.%). Quartz occurs as anhedral (round to lobate) to subhedral crystals and angular crystal fragments. The matrix is fine grained (≤0.3 mm) and mainly composed of devitrified glass shards. The dykes of the Moonamby Dyke Suite (samples GH15, 70, 70B, 92) are up to tens of metres wide, show mostly homogeneous texture and contain medium- to coarse-grained phenocrysts (≤3 cm) of K-feldspar, quartz and minor sodic plagioclase (Fig. 3h). The quartzo-feldspathic groundmass is microcrystalline (grain size ≤50 µm) to micropoikilitic. Quartz phenocrysts are anhedral and deeply embayed (or “vermicular”).

Quartz crystals in the Wheepool Rhyolite and the Waurea Pyroclastics contain glassy melt inclusions, together with crystalline, opaque to granular-textured, semi-opaque inclusions (Fig. 6). Melt inclusions are round to negative-crystal-shaped, mostly 5 to 60 µm in diameter, and exceptionally up to 100 µm. Glass is mostly preserved in relatively small inclusions (<40 µm). Glass is colourless or, in some cases, pink to pale brown. A bubble is present in all inclusions (bubble = 4.6 ±1.5 vol.% n = 16, and 7.0 ±2.2 vol.% n = 20 of the inclusion in the Wheepool Rhyolite and Waurea Pyroclastics, respectively). These are interpreted as shrinkage bubbles, formed during cooling, rather than being droplets of fluid co-trapped with the melt. Mineral phases are only locally present, including K-feldspar and Fe-Ti oxide (identified by SEM-EDS), and a yellow prismatic unidentified mineral. Because of the variable assemblage and crystal/glass ratio, these are interpreted as primary, co-trapped minerals. Some large (>50 µm) opaque melt inclusions have radial cracks, and are surrounded by a corona of small fluid inclusions. These are interpreted as decrepitation cracks, through which fluids expelled from the inclusion upon decompression and crystallisation were injected into the host mineral (Lowenstern, 1995). In contrast with the volcanic units, melt inclusions from the Moonamby Dyke Suite are completely crystalline (Fig. 6a-c), most likely as a consequence of slower cooling. Their shapes vary from round to elongate to subhedral, and their size is up to 60 µm. Multiple melt inclusions can occur in single crystals, either trapped along crystal growth planes (Fig. 6d) or randomly dispersed in the crystal. Melt inclusions along any given growth surface were trapped nearly simultaneously, whereas melt inclusions along different planes or dispersed in the crystal were trapped at different times, and likely at different stages of melt evolution.

Laboratory homogenisation was observed at 1000 – 1050°C in volcanic units (Wheepool Rhyolite and Waurea Pyroclastics), and at lower temperatures (800 – 850°C) in the Moonamby Dyke Suite. Homogenised inclusions (Fig. 6e) appear clear, round to negative crystal-shaped, and locally have irregular, “bumpy” margins. Small melt inclusions (≤20 µm) are the most susceptible to homogenisation, and successfully homogenised inclusions are mostly up to 40 µm in size. Inclusions that failed to homogenise, even at high temperature, are of two types: 1) opaque to semi-opaque, crystalline inclusions, and 2) clear, glassy, two-phase (glass + bubble) inclusions. The former inclusions mostly have radial cracks or are intersected by penetrative fractures. The latter appear intact, have round or subhedral margins, and contain clear, colourless glass, together with one or multiple bubbles. Both groups of inclusions locally contain multiple bubbles protruding into the host mineral (Fig. 6f).

6. Geochemistry: comparison of whole-rock and melt inclusion analyses

Major element oxides (Tables 4 and 5, Fig. 7)

Silica content of the Gawler SLIP ranges between ~51 and 79 wt.%, with a sharp predominance of felsic rocks (dacite and rhyolite are > 90% in outcrop, Allen et al., 2008). The rock compositions are characterised by increasing K_2O (up to 7 – 8 wt.%) with increasing silica, K_2O/Na_2O mostly between 1 and 3 for felsic samples, and low and decreasing CaO (≤ 1 wt.% at SiO_2 ≥ 70 wt.%) and MgO with increasing silica. The rocks are mostly calc-alkalic to alkali-calcic in the modified alkali-lime plot (Frost et al., 2001), have moderate to high $FeO_{tot}/(FeO_{tot} + MgO)$ mol., which crosses the boundary between magnesian and ferroan fields (Frost et al., 2001), and are metaluminous to mildly peraluminous (alumina saturation index ASI = Al/(Na + K + 2Ca) mol ≤1.1 – 1.2). Higher and scattered ASI values are observed in some whole-rock samples. This scatter, together with the high K_2O/Na_2O (> 3) of some samples, can be attributed to alteration and mobilisation of alkalis. In the total alkalis versus silica diagram, whole-rock compositions straddle the line between alkaline and subalkaline fields.

Generally, overlap has been found between melt inclusion and whole-rock analyses for most major element oxides. Melt inclusion analyses have high K_2O (up to 7 – 8 wt.%) and low CaO and MgO (<0.2 and <0.8 wt.%, respectively). However, the decreasing trends with increasing silica of some elements (Na_2O, K_2O, and Al_2O_3) in melt inclusion analyses do not match whole-rock samples, and ASI in melt inclusion analyses does not show a clear trend with increasing silica. For each analysed unit, homogenised melt inclusions have higher average silica contents than non-homogenised inclusions.

Because the melt was saturated with respect to quartz at the moment of entrapment, some degree of post-trapping crystallisation of quartz on inclusion walls can be expected, resulting in decrease of silica in the melt inclusion. Compositional modifications can also be induced by experimental conditions, as host quartz is melted during heating in the laboratory. In general, heating to temperatures lower than the trapping temperature can result in low silica in the melt inclusions, whereas heating to higher temperatures (overheating) will produce artificially high silica values. These processes could explain the wide SiO_2 melt inclusion composition range. Crystallisation and melting of host quartz would also have a “dilution” effect on oxides other than SiO_2, proportional to the amount of quartz crystallised or melted. This effect can be responsible for the decreasing trends of some element oxides in Harker diagrams (e.g. K_2O, Al_2O_3), which represent mixing lines with quartz. Further, a few melt inclusion analyses with SiO_2 <70 wt.% have very high K_2O and Al_2O_3 in comparison with whole-rock analyses (Fig. 7). This is not believed to be due to boundary layer effects, because low SiO_2 would correspond to the highest trace element values, which is not the case. Given the high K_2O and Al_2O_3 of these analyses, this effect may be due to contamination of melt inclusions from a few co-trapped feldspar crystals during heating experiments.

Trace elements (Tables 4 and 5, Figures 8 and 9)

Both whole-rock and melt inclusion analyses indicate high concentrations of rare earth elements (REE), Y, and high field strength elements (HFSE), and low concentrations of Cr and Ni in comparison with average continental crust values (Hu and Gao, 2008). Whole-rock concentrations of REE, Y, and Zr increase with silica and peak at ~70 wt.% SiO_2. Other HFSE (Nb, Ta, and Th) and Rb increase even in the most silica-rich compositions, and for high-silica analyses (>70 wt.%), these trends become sub-vertical. These relationships suggest incompatible behaviour of these elements, even after the magma reached eutectic composition. This is also clear in plots of these incompatible elements versus Al_2O_3 and alkalis (not shown). Whole-rock Sr, Ba, Eu, P, and Ti are negatively correlated with silica, compatible with crystallisation of modal minerals feldspar, apatite, and Fe-Ti oxide.

On trace element variation diagrams, melt inclusions and felsic whole-rock samples plot on similar trends. Primitive mantle-normalised plots of whole-rock and melt inclusion samples (Fig.9) have similar trends with Ba, Sr, Ti, P, and ±Eu negative spikes, and slightly decreasing REE distributions (La_N/Yb_N = 12 ±3.5, n = 12). Melt inclusions are generally lower in compatible elements (Sr, Ba and Eu; elements that have a high distribution coefficient with feldspar; White et al., 2003) and higher in incompatible elements (Th, Nb, Ta, Rb), compared with felsic whole-rock samples. Thus, melt inclusions have generally “more evolved” compositions.

Melt inclusion trace elements have wide compositional ranges, even among inclusions in the same grain. Barium, Th, REE, Zr and Ta can vary by a factor of >3; Nb, Sr and Rb by a factor of 2 – 2.5. The largest ranges were measured for Cu (<9 to 1800 ppm). Although the possibility of contamination exists, laser ablation signals do not indicate significant surface Cu contamination introduced by polishing. A possible cause of Cu contamination can be identified in diffusion in quartz during heating in the laboratory (Kamenetsky and Danyushevsky, 2005), which may have occurred despite wrapping the grains in Pt foil.

Melt inclusions show moderate to good correlation between incompatible elements (Nb-Ta, Nb-Th, Th-Rb are moderately to well correlated, r^2 = 0.5-0.8). Lead, U, and Sn show positive correlations with incompatible elements in melt inclusions, but have a wider scatter in whole-rock analyses. The ratios Th/U and Th/Pb retain near-primitive mantle values (~5, and ~0.5 by weight, respectively) in melt inclusions, but vary significantly in whole-rock samples (Fig. 8).

Volatile components

Melt inclusions have moderate to high F contents (F ≤1.3 wt.%) and low Cl contents (Cl ≤0.2 wt.%) (Table 5, Fig. 7). Broad positive F-Cl correlation exists in melt inclusions from the Wheepool Rhyolite. Chlorine shows a strong positive correlation with incompatible elements, Pb in particular (r^2 = 0.84), except for one analysis. In volcanic samples, broad positive correlation of F with REE, Y, Zr and Hf was also found. Phosphorus and S are consistently below detection limit (~250 and ~200 ppm, respectively for EPMA), in general agreement with the felsic whole-rock data (Table 4).

A fist order estimate of water content can be calculated from the difference between microprobe totals and 100 % (water by difference, H_2O*; Devine et al., 1995). Unheated glassy inclusions, all from the volcanic units, have average H_2O* = 1.6 ±1.3 wt.% (n = 12), whereas inclusions heated in the laboratory have average H_2O* = 1.0 ±0.9 wt.% (n = 39). Melt inclusions from the Moonamby Dyke Suite, all homogenised in the lobaratory, have average H_2O* = 3.1 ±1.0 wt.% (n = 12). Water content of melt inclusions can be modified after entrapment by natural and experimental causes (leakage along microcracks, diffusion through quartz lattice; Lowenstern, 1995; Qin and Anderson, 1992). Thus, unheated inclusions are considered more representative of the original H_2O content. Estimates based on the difference method are also affected by significant analytical error. Microprobe totals of the standard glass analyses are within 1 wt.% uncertainty compared with published values. This uncertainty corresponds to ~40 % of (100 %-total) values of melt inclusions from unheated volcanic units, translating into ~40 % relative error for H_2O* estimates in these samples.

Quartz-hosted, homogenised and unheated melt inclusions from the Eucarro Rhyolite of the upper GRV (McPhie et al., 2011) have very similar major element compositions to the lower GRV melt inclusions (Fig. 7). These inclusions are up to 100 µm in size, round to euhedral negative-shaped, and homogenised at ~850°C. The upper GRV melt inclusions and whole-rock samples have similarly high K_2O (up to ~7 wt.%) and K_2O/Na_2O (> 1), and low CaO (<1 wt.%), Ni, and Cr compared to the lower GRV; REE, Y, HFSE and

FeO_{tot}/(FeO_{tot} + MgO) are higher at any given SiO_2 value (Tables 4 and 5, Figures 7 and 8). Trace element Harker diagrams (e.g. Th, Rb, Zr) indicate broader fractionation trends (i. e. larger scatter at any SiO_2 value) for the lower GRV than the upper GRV. This has been interpreted as indicative of multiple lines of descent in the lower GRV, representative of different magma batches (Stewart, 1994). Melt inclusions from the upper GRV have very similar F contents to the lower GRV (≤1.3 wt.%) and slightly higher Cl contents (≤0.4 wt.%). The difference between EPMA totals and 100 % in upper GRV melt inclusions averages 98.5 ±1.4 wt.% (n = 47), largely overlapping the lower GRV.

Zircon saturation and magma temperature estimates

The ratio Zr/Hf remains nearly constant (Zr/Hf ~40) as Zr increases with increasing silica for SiO_2 ≤70 wt.%, and decreases with decreasing Zr in both whole-rock samples with SiO_2 ≥70 wt.% and melt inclusions (Fig. 8). This Zr trend is interpreted as indicative of zircon saturation and zircon crystallisation at SiO_2 ≥70 wt.%, accompanied by Zr-Hf fractionation (Linnen and Keppler, 2002; Thomas et al., 2002). Zircon solubility in silicate melts is strongly dependent on temperature (Rubatto and Hermann, 2007; Watson and Harrison, 1983). Application of the zircon saturation model (Watson and Harrison, 1983) to whole-rock samples with SiO_2 ≥70 wt.% and melt inclusions yields temperatures of 782 – 909°C (Tables 4 and 5) if one melt inclusion analysis with anomalously low Zr content is excluded. Peak temperature corresponds to 470 ppm Zr, although Zr concentrations as high as 680 ppm have been measured in the lower GRV (Giles, 1988; Stewart, 1994), translating into T = 945°C. For upper GRV melt inclusions, temperatures of T = 853 – 913°C can be calculated. This method takes into consideration the effect of network modifying components by means of the parameter M = (Na + K + 2Ca)/(Al · Si). Therefore, samples that show mobilisation of alkalis (low Na_2O ~1 wt.%, K_2O/Na_2O > 5) have been discarded when calculating zircon saturation temperatures. It should be noted, however, that F can increase the solubility of some HFSE in silicate melts, including Zr (Keppler, 1993), and potentially affect temperature estimates based on zircon solubility. Despite the uncertainties of the method, these temperatures partially overlap with available estimates for the upper GRV based on the equilibrium pigeonite-augite, which yield temperatures of 900 – 1100°C (Creaser and White, 1991; Stewart, 1994).

Comparison with other SLIP

Comparison of the GRV as a whole with other SLIP and large felsic volcanic units indicates compositional similarities (Fig. 10). In particular, for the compared provinces, K_2O mostly plots between high-K and ultra-K, and Zr increases with increasing SiO_2 and peaks around SiO_2 = 70 wt.%, with Zr concentrations well in excess of 500 ppm in the Etendeka and Snake River Plain provinces (Christiansen and McCurry, 2008; Marsh et al., 2001). All the compared provinces either plot in the ferroan field, or are transitional between ferroan and magnesian fields of Frost et al. (2001). High field strength elements, HREE, and Rb are enriched, whereas Sr is depleted, in comparison to the upper continental crust. In some of these provinces (Etendeka, Snake River Plain, Keweenawan, and GRV), phenocryst assemblages are mostly anhydrous (augite ± pigeonite are the common ferromagnesian minerals, whereas biotite and amphibole are scarce to absent), and estimated temperatures are higher than for most felsic rocks (up to > 1000°C, Table 1). These provinces are either dominated by large felsic lavas, or composed of both lavas and rheomorphic pyroclastic flows. Conversely, the Whitsunday Prince and the Sierra Madre Occidental, which are dominated by pyroclastic flow deposits, have lower Zr contents, and generally lower $FeO_{tot}/(FeO_{tot} + MgO)$. In the Nb vs Y plot (Pearce et al., 1984), the compared rocks are transitional between the volcanic arc-collisional granite and within plate fields, and in the Nb vs 10000 · Ga/Al plot (Whalen et al., 1987), are transitional between I-type and A-type. The upper GRV melt inclusions and whole-rock samples plot in the within-plate field of tectonic environment discrimination diagrams (Pearce et al., 1984), and in the A-type field in terms of HFSE and Ga/Al (Collins et al., 1982; Whalen et al., 1987), whereas the lower GRV are transitional between the volcanic arc and within-plate fields, and between I- and A-type fields. Significant, although unconstrained, F contents have been inferred for the Keweenawan Midcontinent Rift volcanic units (Green and Fitz, 1993).

7. Discussion

7.1 Representativity of melt inclusion data

Melt inclusions can be affected by several processes that could limit their usefulness as indicators of melt composition. The effects of these processes should be assessed before analytical data are used. Accumulation of elements incompatible with the host mineral during its growth (boundary layer effect; Baker, 2008; Lowenstern, 1995) is inversely correlated with element diffusivity in the silicate melt, and can result in anomalously high element concentrations in melt inclusions in comparison with matrix glass. In the GRV melt inclusions, high concentrations of some trace elements alone (e.g. Th, Nb, Ta) could be attributed to boundary layer effect, however, the concurrent low concentrations of Sr, Ba and Eu (Figures 8 and 9) argue against this hypothesis. All these elements are incompatible with quartz, and would be increased to a different extent by boundary layer effects around crystallising quartz. Plots of compatible versus incompatible elements (e.g. Sr vs Nb, Sr vs Rb, Ba vs Th) describe similar trends in whole-rock and melt inclusion analyses, consistently with fractionation of modal minerals. This suggests that, if boundary layer effect occurred, it did not affect trace element contents significantly.

Wide variation of silica content between unheated and homogenised inclusions suggests post-entrapment crystallisation and/or re-melting of host quartz during heating experiments. Some melt inclusions have significantly higher SiO_2 values (>80 wt.%) in comparison with whole-rock analyses. These values can be interpreted as due to melting of host quartz during heating experiments. Silica contents up to ~80 wt.% of homogenised melt inclusions are in broad agreement with the groundmass compositions, as inferred by simple mass-balance considerations. Consider for example the Wheepool Rhyolite, which has whole-rock composition of SiO_2 = 78 wt.% (sample GH06, Table 4), with 10 vol.% feldspar content (SiO_2 = 65 wt.%), and 1 vol.% quartz. Under these conditions, a SiO_2 content of ~80 wt.% can be calculated for the groundmass. For the Wheepool Rhyolite, homogenised melt inclusions have average SiO_2 = 78.5 ±1.3 wt.%, 6.44 wt.% (or 8.1 % relative) higher than unheated melt inclusions. This variation is reflected on concentrations of other elements and on trends in Harker diagrams.

Although caution is due because of the aforementioned analytical and experimental effects, we consider melt inclusion compositions as indicative of the melt composition in the crystallisation interval of quartz phenocrysts.

7.2 The effects of magmatic processes and rock alteration on composition

In ancient rocks, alteration introduces uncertainty in the interpretation of whole-rock geochemical data. The GRV show evidence of weak but widespread alteration of feldspar to sericite and brick-red, probably cooling-related, groundmass oxidation. Because of this alteration, whole-rock data, particularly the most “mobile” elements (Na, K), should be considered carefully.

Melt inclusion and whole-rock analyses show relatively good overlap for most “mobile”, water-soluble oxides (Na_2O, K_2O, CaO) (Tables 4 and 5, Fig. 7). Similarity between whole-rock and melt inclusion analyses suggests that alteration has not systematically and significantly affected the whole-rock content of alkalis. However, some whole-rock samples have scattered alkalis and ASI values, which can be attributed to local rock alteration (e.g. low Na whole-rock content of the Waurea Pyroclastics, sample GH13, Table 4, Fig. 7). A relative scatter of melt inclusion ASI was also observed. Because ASI values of unheated and heated melt inclusions overlap, this is not attributed to heating in the laboratory, and can tentatively be ascribed to different levels of remobilisation of alkalis during EPMA analysis.

The wide variations measured in melt inclusion trace element compositions cannot be explained by quartz dilution and boundary layer effects. Geochemical modelling of melt inclusion data indicates that variations in compatible and incompatible trace elements can be explained by extensive fractional crystallisation (~80% crystallisation, Fig. 11).

This would imply the presence of significant volumes of cumulates. Potentially, the voluminous HS plutons could represent crystal-rich mushes, from which felsic melt could have been extracted. From a geochemical point of view, the cumulate should have complementary characteristics to the melt. However, primitive mantle-normalised plots (Fig. 10) indicate that the HS granite has similar compositional characteristics to the volcanic units and dykes, making it an unlikely candidate as cumulitic rock.

A second mechanism– partial remelting of crystallised magma – can be envisaged, and can be modelled as fractional melting of HS granite. This hypothesis seems to be substantiated by field and petrographic evidence, given the occurrence of felsic enclaves, or partially melted granite blocks. This hypothesis would also help explain why some melt inclusions have more evolved compositions than whole-rock samples. This is inconsistent with fractionation, which would lead to increase in incompatible elements and decrease of compatible elements in the most evolved melts, represented by groundmass or whole-rock. Processes of re-melting of crystallised portions of the magma chamber have been proposed for several large intermediate to felsic systems (Bachmann et al., 2002; Murphy et al., 2000). Under these conditions, melt inclusions may not represent a continuous sampling of evolving melt. The two mechanisms are not mutually exclusive, and might have occurred together.

Some trace elements, U, Pb and Sn in particular, show good correlation with Th in melt inclusions, indicating incompatible behaviour, but are scattered and variably depleted in whole-rock analyses compared to melt inclusions (e.g. Th vs U, Fig. 8). This depletion is reflected in the locally high whole-rock Th/U and Th/Pb and suggests late mobility of these elements.

Geochemical studies of igneous rocks hosting U mineralisation (Chabiron et al., 2001; Gray et al., 2011) have also found similar relationships between melt inclusion and whole-rock samples. Solubility of U and Sn in Cl-F-CO_2-bearing aqueous fluids at relatively oxidising conditions has been experimentally demonstrated (Bali et al., 2011; Keppler and Wyllie, 1991), whereas Th solubility seems less affected by variations of these parameters. Evidence of late-stage exsolution of a F-CO_2-bearing fluid has been found in rhyolite samples in both the Glyde Hill and the Chitanilga Volcanic Complexes in the form of pockets of H_2O-F-CO_2-bearing minerals (micro-miaroles and amygdales; Agangi et al., 2010). These fluids may be responsible for the differences between whole-rock and melt inclusion trace element data. We hypothesise that Th, Pb, U, and Sn mostly behaved as incompatible elements during magmatic fractionation, resulting in increased concentrations and in linear correlations, and near-primitive-mantle Th/U and Th/Pb ratios in the melt. Syn- to post-magmatic processes involving fluid leaching of ore metals resulted in preferential transport and depletion of U, Pb, and Sn relative to Th in the lower GRV.

7.3 Magma volatile content

Melt inclusion analyses indicate positive correlation between Cl and incompatible elements (Pb, Rb, U, Th). Experiments on element partitioning between silicate melt and aqueous fluid have shown that Cl is highly volatile and strongly partitions into the fluid phase in equilibrium with the melt (Carroll and Webster, 1994). Thus, we interpret the observed correlation as a geochemical indication that the GRV melt was volatile-undersaturated during crystallisation of quartz. The patterns shown by F are somewhat more complex and could be due to fractionation of F-bearing minerals, such as F-apatite and fluorite from the melt. Evidence for the crystallisation of magmatic fluorite (fluorite daughter crystals in melt inclusions, and quartz-hosted fluorite inclusions) were found in the upper GRV (McPhie et al., 2011). Lower GRV samples presented here do not show such textural evidence, although several melt inclusions plot above fluorite saturation at 800˚C in the F vs Ca plot (Fig. 7) (Dolejš and Baker, 2006), thus providing support for melt saturation with respect to fluorite. However, generally incompatible behaviour of F is expected. Many melt inclusion analyses indicate that F/CaO (wt.%) in the melt was >0.68, or F_2/Ca (mol) >1. For these compositions, crystallisation of fluorite will not buffer F, which is expected to increase with progressing crystallisation (Dolejš and Baker, 2006).

The higher microprobe totals in heated inclusions can be explained by diffusion of H_2 out of the inclusions through the host mineral lattice or H_2O loss along microcracks during heating experiments (Qin and Anderson, 1992). Therefore, calculated H_2O concentrations of homogenised melt inclusion (H_2O^* = 1.0 wt.% for the volcanic units and = 3.1 wt.% for the dykes) might be underestimated to some extent. Available melt inclusion data on the upper GRV (Eucarro Rhyolite; McPhie et al., 2011) also indicate high concentrations of F (≤1.3 wt.%), moderate Cl (≤0.4 wt.%), and high microprobe totals (average 98.5 wt.%) for unheated melt inclusions.

Volatile-undersaturation and low H_2O content of the melt are in agreement with the observed anhydrous parageneses observed in the lower GRV (Table 3) and upper GRV (Giles, 1988). Primary ferromagnesian mineral phases in the volcanic units are anhydrous, dacite and andesite units contain well-preserved clinopyroxene, and no amphibole or biotite are present. Biotite only occurs in interstitial position in the HS granite. Previous estimates of water content in GRV magmas based on paragenesis (method of Nekvasil, 1988) indicated a H_2O content of 1 – 2 wt.% (Creaser and White, 1991).

7.4 Eruption and emplacement mechanisms

7.4.1 Distinguishing felsic lavas from ignimbrites

Because of the different eruption and emplacement mechanisms, most lavas and pyroclastic flow deposits are readily distinguished on the basis of textures and geometry of the units. Rhyolitic lavas are usually <1 km^3 in volume, and typical aspect ratios for felsic lavas and domes are between 1:1 and 1:100 (Henry et al., 1988; Walker, 1973). Typical outcrop characteristics of lavas include flow folds and flow bands, elongate vesicles, autobreccia, and vesicular-pumiceous exterior around a non-vesicular interior (Fink and Manley, 1987; Henry et al., 1988; McPhie, 1993). At the microscale, even distribution of phenocrysts, paucity of broken crystals, and microcrystalline or glassy matrix are considered as indicative of lavas (Bonnichsen and Krauffman, 1987; Allen and McPhie, 2003). Recognition of large, low-aspect ratio felsic lavas has been relatively recent (Bonnichsen and Krauffman, 1987; Green and Fitz, 1993; Twist and French, 1983), and until then extensive felsic units were assumed to be of pyroclastic origin.

Ignimbrites can be very large (hundreds of km^3), and have aspect ratios typically in the range 1:100 to 1:1000, and occasionally much lower (Walker, 1980; Wilson et al., 1995). Diagnostic features of ignimbrites include abundant broken crystals, lithic fragments and glass shards (Henry et al., 1988; 1990; Henry and Wolff, 1992). Phenomena of welding (coalescence of juvenile components) and welding compaction can occur in ignimbrites, depending on the viscosity of the juvenile component, ratio between juvenile and non-juvenile components, and thickness of the deposit. A complete spectrum exists between low-grade, non-welded to high-grade, welded ignimbrites (Wright et al., 1980; Wolff and Wright, 1981; Walker, 1983). High and extremely high grade ignimbrites record a transition between particulate and non-particulate flow. As a result of viscous flow, the deposits can mimic textures of lavas (Andrews et al., 2008; Branney et al., 2004; Branney and Kokelaar, 1992). True lavas have been distinguished from extremely high grade (lava-like) ignimbrites based on combinations of characteristics, namely lack of lithic and pumice fragments, and steep flow bands, whereas ignimbrites may show local preservation of pyroclastic texture or gradation from coherent to clastic texture (Branney et al., 1992; 2008; Branney and Kokelaar, 2003). Welded pyroclastic flow deposits may also have vertical zoning of phenocryst abundance, an indication of deposition from granular fluid-based pyroclastic density currents (Branney and Kokelaar, 2003; Branney at al, 2008).

The widespread extent and low aspect ratio of some felsic units in the GRV lead some authors to interpret these rocks as ignimbrites in which intense welding had obliterated textural evidence of a fragmental origin (Blissett, 1985; Giles, 1977). However, several lines of evidence suggest that these units were probably emplaced as lavas. This conclusion is based on the evenly porphyritic texture, microcrystalline groundmass, deformation structures indicative of non-particulate flow such as flow bands and lineations, presence and distribution of thick breccia domains (autobreccia), elongate vesicles/amygdales, lack vitriclastic texture and lack or very local presence of fiamme, and paucity of fractured crystals. The very local presence of fiamme at the base of the Yantea Rhyolite-dacite can result from incorporation of pumice in the flow, or welding of clasts in basal autobreccia, and their presence does not disprove emplacement of a unit as lava (Bull and McPhie, 2007; Manley, 1996). Another distinctive characteristic pointing to an effusive eruptive mechanism is the near-absence of broken crystals. Conversely, pyroclastic flow deposits contain a moderate amount of crystal fragments, even in welded domains where microtextural evidence of fragmental origin is not preserved (Fig. 5b).

The presence of medium-coarse grained felsic igneous enclaves also supports effusive eruption. These enclaves show evidence for partial melting (anhedral K-feldspar and amoeboid quartz crystals surrounded by fine grained groundmass) and subsequent quenching (microcrystalline groundmass, granophyric rims around K-feldspar, Fig. 4). Quenching textures indicate moderate to high degrees of undecooling, and likely recorded temperature decrease accompanying eruption. Close compositional similarities with HS and felsic GRV samples (Fig. 9, Table 4) suggest that the enclaves originated from partial melting of previously crystallised GRV-HS magma, such as the solid margins of the magma chamber or largely solid crystal mushes. Textures imply limited disaggregation, and appear to be inconsistent with an explosive eruption mechanism. Stoped blocks from the margin and top of the magma chamber would have been nearly buoyant in the magma, and easily entrained during magma withdrawal.

Similar considerations and interpretations have been proposed for the Yardea Dacite and Eucarro Rhyolite of the upper GRV (Garner and McPhie, 1999; Morrow and McPhie, 2000; Allen and McPhie, 2002; Allen et al., 2003; McPhie et al., 2008). Other units (e.g. the Lake Gairdner Rhyolite) can be confidently interpreted as ignimbrites on the basis of the vitriclastic texture, presence of fiamme, and moderate amount of crystal fragments (Figures 3g, and 5a, b).

7.4.2 Eruption and emplacement of extensive felsic lavas

The eruption and emplacement mechanisms of volcanic units are determined by the interplay of several parameters, including magma bulk composition, volatile content, temperature, total volume erupted, and eruption rate. Bulk composition, temperature, crystal and bubble content, and dissolved volatile components are important controls on viscosity, which critically affects the eruption mechanism (Bottinga et al., 1995; Dingwell, 1996). The role of volatile components – H_2O and F in particular – in depolymerising and reducing the viscosity of silicate melts is well established (Dingwell and Mysen, 1985; Dingwell et al., 1985; Giordano et al., 2004; Holtz et al., 1999; Manning, 1981). Small variations in the concentration of these volatiles can generate large, non-linear variations in melt viscosity (Dingwell et al., 1985; Dingwell, 1996; Giordano et al., 2008). The effect of other volatile species (CO_2, Cl, S) on viscosity is less well constrained (Dingwell and Hess, 1998). Volatile components also play a fundamental role in triggering volcanic explosions through exsolution of a fluid phase and vesiculation of magma. An important difference between water and F is that the latter is more melt-compatible, and has a lower tendency to exsolve into a fluid phase in equilibrium with the melt (Webster, 1990).

Magmatic temperatures in the GRV are believed to have been high; zircon saturation in the lower GRV indicates temperature up to ~950°C, and pyroxene geothermometry in the upper GRV indicates temperatures of 900 – 1100°C (Creaser and White, 1991; Stewart, 1994). Viscosity calculations for the Yardea Dacite indicate that these high temperatures, together with estimated water contents of 1 – 2 wt. %, and an average F content of ~0.16 wt. %, could have promoted a largely effusive behaviour (Pankhurst et al., 2011). These calculations are based on whole-rock F contents, which are higher than upper continental crust by a factor of 3 to 5 (Wedepohl, 1995), but which clearly represent underestimates of the original melt F content as indicated by melt inclusions. High F contents would have caused further viscosity reduction. Thus, high concentrations of de-polymerising and viscosity-reducing F of the GRV, coupled with high temperature and large volumes erupted, created the favourable conditions for large-volume effusive eruptions. The probable low water concentrations would have caused low degree of vesiculation and low explosivity during eruption. Large volumes of magmas (up to several hundreds of km^3) were erupted mostly non-explosively, and high eruption rate allowed the lava to spread widely (several tens of km).

Significant amounts of F, high F/Cl, water-undersaturated compositions, and high magmatic temperatures have been inferred in the source magmas of other extensive felsic lavas and strongly rheomorphic ignimbrites of similar geodynamic setting and geochemical characteristics (Snake River Plain-Yellowstone, Christiansen and McCurry, 2008; Keweenawan Midcontinent Rift volcanic units, Green and Fitz, 1993; Etendeka Igneous Province, Namibia, Ewart et al., 1998b; 2004).

8. Conclusions

The GRV and HS granite represent a Mesoproterozoic SLIP (the Gawler SLIP) with a total volume of ~100 000 km^3 or more (Blissett et al., 1993). The GRV are dominated by felsic lava units (>90 vol.%), and also include minor ignimbrites and intermediate to mafic lavas. The Glyde Hill and Chitanilga Volcanic Complexes are the best exposed successions of the lower GRV, and include several moderately extensive and voluminous felsic units (≤170 km^3), and thick but localised mafic-intermediate lavas. Meso- and micro-scale textures suggest that most felsic units were emplaced as lavas that were able to flow for long distances (flood rhyolites). These characteristics include even porphyritic textures, indicators of viscous flow deformation (autobreccia, flow bands, elongate vesicles), and lack of fractured crystals and vitriclastic texture. The volcanic sequence was intruded by cogenetic granite and numerous porphyritic rhyolitic dykes.

Whole-rock and melt inclusion analyses in the lower GRV, and comparison with the upper GRV show that the GRV melt had high K_2O (up to 7-8 wt.%), high K_2O/Na_2O (> 1), high F (≥1.3 wt.%) concentrations throughout and was metaluminous to weakly peraluminous (ASI ≤1.1 – 1.2). Rare earth elements, HFSE, Y, Ga, and $FeO_{tot}/(FeO_{tot}+MgO)$ are moderate to high in comparison with felsic continental crust, especially in the upper GRV. Concentrations of trace elements compatible with feldspar are low (Sr ≤160 ppm, Ba ≤1870 ppm, and Eu <3 ppm for SiO_2 ≥ 70 wt.%), and incompatible elements are high (Th ≤50 ppm, Rb ≤800 ppm, Nb ≤45 ppm), especially in melt inclusions. Overall, geochemical characteristics are consistent with protracted crystallisation of the modal mineral assemblages (feldspar, ±quartz, ±clinopyroxene, apatite, zircon, Fe-Ti oxide).

Similarity of whole-rock and melt inclusion compositions suggests that, despite the Mesoproterozoic age, most major and trace elements have not been substantially modified by alteration, and whole-rock analyses can be considered as indicative of the magma composition. Notable exceptions are the low alkalis in some samples (reflected in high ASI > 1.2), and Pb, U and Sn, which were selectively mobilised and variously depleted. Alteration of Pb, U and Sn is evident from relatively low and scattered whole-rock compositions and lack of correlation between these elements and other incompatible elements (e.g. Th), whereas melt inclusion plots show good correlations, indicating incompatible behaviour. Mobilisation of Pb, U, and Sn may have occurred at late- to post-magmatic stages by means of a F-bearing fluid.

The combination of high concentrations of viscosity-reducing F in the melt, together with high magmatic temperatures (≤950°C zircon saturation temperature; 900-1100°C pyroxene thermometry; Creaser and White, 1991), would have favoured low explosivity and effusive behaviour during eruption of the GRV. These features help explain the abundance of extensive felsic lavas in the Gawler SLIP.

Acknowledgments

This research was funded by ARC-CODES grants to the authors. Field and logistical support was provided by the Primary Industries and Resources of South Australia (PIRSA, particularly Martin Fairclough and Stacey Curtis). Dr. Karsten Gömann, Philip Robinson and Katie McGoldrick (University of Tasmania) are thanked for analytical assistance. Notes provided by the three anonymous reviewers significantly improved the manuscript.

References

Agangi, A., Kamenetsky, V.S., McPhie, J., 2010. The role of fluorine in the concentration and transport of lithophile trace elements in felsic magmas: Insights from the Gawler Range Volcanics, South Australia. Chemical Geology 273, 314-325.

Agangi, A., McPhie, J., K.amenetsky, V.S., 2011. Magma chamber dynamics in a silicic LIP revealed by quartz: the Mesoproterozoic Gawler Range Volcanics. Lithos 126, 68-83.

Allen, S.R., McPhie, J., 2002. The Eucarro Rhyolite, Gawler Range Volcanics, South Australia: a > 675 km^3, compositionally zoned lava of Mesoproterozoic age. Geological Society of America Bulletin 114, 1592-1609.

Allen, S.R., McPhie, J., Ferris, G., Simpson, C., 2008. Evolution and architecture of a large felsic igneous province in western Laurentia: The 1.6 Ga Gawler Range Volcanics, South Australia. Journal of Volcanology and Geothermal Research 172, 132-147.

Allen, S.R., Simpson, C.J., McPhie, J., Daly, S.J., 2003. Stratigraphy, distribution and geochemistry of widespread felsic volcanic units in the Mesoproterozoic Gawler Range Volcanics, South Australia. Australian Journal of Earth Sciences 50, 97-112.

Anderson, J.L., Morrison, J., 2005. Ilmenite, magnetite, and peraluminous Mesoproterozoic anorogenic granites of Laurentia and Baltica. Lithos 80, 45-60.

Andrews, G.D.M., Branney, M.J., Bonnichsen, B., McCurry, M., 2008. Rhyolitic ignimbrites in the Rogerson Graben, southern Snake River Plain volcanic province: volcanic stratigraphy, eruption history and basin evolution. Bulletin of Volcanology 70, 269-291.

Bachmann, O., Dungan, M.A., Lipman, P.W., 2002. The Fish Canyon magma body, San Juan volcanic field, Colorado: Rejuvenation and eruption of an upper-crustal batholith. Journal of Petrology 43, 1469-1503.

Baker, D., 2008. The fidelity of melt inclusions as records of melt composition. Contributions to Mineralogy and Petrology 156, 377-395.

Bali, E., Audétat, A., Keppler, H., 2011. The mobility of U and Th in subduction zone fluids: an indicator of oxygen fugacity and fluid salinity. Contributions to Mineralogy and Petrology 161, 597-613.

Betts, P.G. Giles, D., Foden, J., Schaefer, B.F., Mark, G., Pankhurst, M.J., Forbes, C.J., Williams, H.A., Chalmers, N.C., Hills, Q., 2009. Mesoproterozoic plume-modified orogenesis in eastern Precambrian Australia. Tectonics 28, TC3006.

Betts, P.G., Giles, D., 2006. The 1800-1100 Ma tectonic evolution of Australia. Precambrian Research 144, 92-125.

Betts, P.G., Giles, D., Lister, G.S., Frick, L.R., 2002. Evolution of the Australian lithosphere. Australian Journal of Earth Sciences 49, 661-695.

Betts, P.G., Giles, D., Schaefer, B.F., Mark, G., 2007. 1600–1500Ma hotspot track in eastern Australia: implications for Mesoproterozoic continental reconstructions. Terra Nova 19, 496-501.

Blissett, A.H., 1975. Rock units in the Gawler Range Volcanics, South Australia. Geological Survey of South Australia, Quarterly Geological Notes 55, 2-14.

Blissett, A.H., 1977a. CHILDARA, Sheet SH/53-14, 1:250000 geological series. Geological Survey of South Australia, Adelaide.

Blissett, A.H., 1977b. GAIRDNER, Sheet SH/53-15, 1:250000 geological series. Geological Survey of South Australia, Adelaide.

Blissett, A.H., Creaser, R.A., Daly, S.J., Flint, R.B., Parker, A.J., 1993. Gawler Range Volcanics. In: J.F. Drexel, Preiss, W. V., Parker, A. J. (Editor), The Geology of South Australia. Geological Survey of South Australia, Adelaide.

Bonnichsen, B., Kauffman, D.F., 1987. Physical features of rhyolite lava flows in the Snake River Plain volcanic province, Southwestern Idaho. Geological Society of America 212 (Special Paper), 119-145.

Bottinga, Y., Richet, P., Sipp, A., 1995. Viscosity regimes of homogeneous silicate melts. American Mineralogist 80, 305-318.

Branch, C.D., 1978. Evolution of the middle Proterozoic Chandabooka Caldera, Gawler range acid volcano-plutonic province, South Australia. Journal of the Geological Society of Australia 25, 199-216.

Branney, M.J., Barry, T.L., Godchaux, M., 2004. Sheathfolds in rheomorphic ignimbrites. Bulletin of Volcanology 66, 485-491.

Branney, M.J., Bonnichsen, B., Andrews, G.D. M., Ellis, B., Barry, T.L., McCurry, M., 2008. 'Snake River (SR)-type' volcanism at the Yellowstone hotspot track: distinctive products from unusual, high-temperature silicic super-eruptions. Bulletin of Volcanology 70, 293-314.

Branney, M.J., Kokelaar, B.P., 2003. Pyroclastic density currents and the sedimentation of ignimbrites. Geological Society London Memoirs, pp. 152.
Branney, M.J., Kokelaar, B.P., McConnell, B.J., 1992. The Bad Step Tuff - a lava-like rheomorphic ignimbrite in a calc-alkaline piecemeal caldera, English Lake District. Bulletin of Volcanology 54, 187-199.
Branney, M.J., Kokelaar, P., 1992. A reappraisal of ignimbrite emplacement - Progressive aggradation and changes from particulate to nonparticulate flow during emplacement of high-grade ignimbrite. Bulletin of Volcanology 54, 504-520.
Bryan, S.E., 2007. Silicic large igneous provinces. Episodes 30, 20-31.
Bryan, S.E., Ernst, R.E., 2008. Revised definition of large igneous provinces (LIPs). Earth-Science Reviews 86, 175-202.
Bryan, S.E., Ewart, A., Stephens, C.J., Parianos, J., Downes, P.J., 2000. The Whitsunday Volcanic Province, Central Queensland, Australia: lithological and stratigraphic investigations of a silicic-dominated large igneous province. Journal of Volcanology and Geothermal Research 99, 55-78.
Bryan, S.E., Ferrari, L., Reiners, P.W., Allen, C.M., Petrone, C.M., Ramos-Rosique, A., Campbell, I.H., 2008. New insights into crustal contributions to large-volume rhyolite generation in the mid-Tertiary Sierra Madre Occidental province, Mexico, revealed by U-Pb geochronology. Journal of Petrology 49, 47-77.
Bryan, S.E., Riley, T.R., Jerram, D.A., Leat, P.T., Stephens, C.J., 2002. Silicic volcanism: an under-valued component of large igneous provinces and volcanic rifted margins. In: M.A. Menzies, Klemperer, S.L., Ebinger, C.J., Baker, J. (Editor), Magmatic Rifted Margins. Geological Society of America, Special Papers, pp. 99-120.
Budd, A.R., Fraser, G.L., 2004. Geological relationships and Ar-40/Ar-39 age constraints on gold mineralisation at Tarcoola, central Gawler gold province, South Australia. Australian Journal of Earth Sciences 51, 685-699.
Bull, K.F., McPhie, J., 2007. Fiamme textures in volcanic successions: Flaming issues of definition and interpretation. Journal of Volcanology and Geothermal Research 164, 205-216.
Cameron, M., Bagby, W.C., Cameron, K.L., 1980. Petrogenesis of voluminous mid-tertiary ignimbrites of the Sierra-Madre Occidental, Chihuahua, Mexico. Contributions to Mineralogy and Petrology 74, 271-284.
Carroll, M.R., Webster, J.D., 1994. Solubilities of sulfur, noble-gases, nitrogen, chlorine, and fluorine in magmas. Reviews in Mineralogy 30, 231-279.
Chabiron, A., Alyoshin, A.P., Cuney, M., Deloule, E., Golubev, V.N., Velitchkin, V.I., Poty, B., 2001. Geochemistry of the rhyolitic magmas from the Streltsovka caldera (Transbaikalia, Russia): a melt inclusion study. Chemical Geology 175, 273-290.
Christiansen, E.H., McCurry, M., 2008. Contrasting origins of Cenozoic silicic volcanic rocks from the western Cordillera of the United States. Bulletin of Volcanology 70, 251-267.
Coffin, M.F., Eldholm, O., 1994. Large igneous provinces - Crustal structure, dimensions, and external consequences. Reviews of Geophysics 32, 1-36.
Collins, W.J., Beams, S.D., White, A.J.R., Chappell, B.W., 1982. Nature and origin of A-type granites with particular reference to southeastern Australia. Contributions to Mineralogy and Petrology 80, 189-200.
Creaser, R.A., 1995. Neodymium isotopic constraints for the origin of Mesoproterozoic felsic magmatism, Gawler-Craton, South Australia. Canadian Journal of Earth Sciences 32, 460-471.
Creaser, R.A., Cooper, J.A., 1993. U-Pb geochronology of Middle Proterozoic felsic magmatism surrounding the Olympic Dam Cu-U-Au-Ag and Moonta Cu-Au-Ag deposits, South Australia. Economic Geology 88, 186-197.
Creaser, R.A., White, A.J.R., 1991. Yardea Dacite - large-volume, high-temperature felsic volcanism from the Middle Proterozoic of South-Australia. Geology 19, 48-51.
Devine, J.D., Gardner, J.E., Brack, H.P., Layne, G.D., Rutherford, M.J., 1995. Comparison of microanalytical methods for estimating H_2O contents of silicic volcanic glasses. American Mineralogist 80, 319-328.
Dingwell, D.B., 1996. Volcanic dilemma-Flow or blow? Science 273, 1054-1055.

Dingwell, D.B., Hess, K.U., 1998. Melt viscosities in the system Na-Fe-Si-O-F-Cl: Contrasting effects of F and Cl in alkaline melts. American Mineralogist 83, 1016-1021.
Dingwell, D.B., Mysen, B.O., 1985. Effects of water and fluorine on the viscosity of albite melt at high-pressure - a preliminary investigation. Earth and Planetary Science Letters 74, 266-274.
Dingwell, D.B., Scarfe, C.M., Cronin, D.J., 1985. The effect of fluorine on viscosities in the system Na_2O-Al_2O_3-SiO_2 - Implications for phonolites, trachytes and rhyolites. American Mineralogist 70, 80-87.
Dolejš, D., Baker, D.R., 2006. Fluorite solubility in hydrous haplogranitic melts at 100 MPa. Chemical Geology 225, 40-60.
Ernst, R.E., Buchan, K.L., Campbell, I.H., 2005. Frontiers in large igneous province research. Lithos 79, 271-297.
Ewart, A., Marsh, J.S., Milner, S.C., Duncan, A.R., Kamber, B.S.,III, Armstrong, R.A., 2004. Petrology and geochemistry of Early Cretaceous bimodal continental flood volcanism of the NW Etendeka, Namibia. Part 2: Characteristics and petrogenesis of the high-Ti latite and high-Ti and low-Ti voluminous quartz latite eruptives. Journal of Petrology 45, 107-138.
Ewart, A., Milner, S.C., Armstrong, R.A., Duncan, A.R., 1998a. Etendeka volcanism of the Goboboseb Mountains and Messum Igneous Complex, Namibia. Part I: Geochemical evidence of early cretaceous Tristan plume melts and the role of crustal contamination in the Paraná-Etendeka CFB. Journal of Petrology 39, 191-225.
Ewart, A., Milner, S.C., Armstrong, R.A., Duncan, A.R., 1998b. Etendeka volcanism of the Goboboseb Mountains and Messum Igneous Complex, Namibia. Part II: Voluminous quartz latite volcanism of the Awahab Magma System. Journal of Petrology 39, 227-253.
Fanning, C.M., Flint, R.B., Parker, A.J., Ludwig, K.R., Blissett, A.H., 1988. Refined Proterozoic evolution of the Gawler Craton, South-Australia, through U-Pb zircon geochronology. Precambrian Research 40-1, 363-386.
Ferrari, L., Lopez-Martinez, M., Rosas-Elguera, J., 2002. Ignimbrite flare-up and deformation in the southern Sierra Madre Occidental, western Mexico: Implications for the late subduction history of the Farallon plate. Tectonics 21, 17-1-17-24.
Ferris, G., 2003. Volcanic textures within the Glyde Hill Volcanic Complex. Quarterly Earth Resources Journal of Primary Industries and Resources, South Australia 29, 36-41.
Fink, J. H., Manley, C. R., 1987. Origin of pumiceous and glassy textures in rhyolite flows and domes. Geological Society of America Special Paper 212, 77-88.
Flint, R.B., 1993. Hiltaba Suite. In: J.F. Drexel, Preiss, W.V., Parker, A.J. (Editor), The geology of South Australia. Geological Survey of South Australia, Adelaide, pp. 127-131.
Fraser, G.L., Skirrow, R.G., Schmidt-Mumm, A., Holm, O., 2007. Mesoproterozoic gold in the central Gawler craton, South Australia: Geology, alteration, fluids, and timing. Economic Geology 102, 1511-1539.
Frost, B.R., Barnes, C.G., Collins, W.J., Arculus, R.J., Ellis, D.J., Frost, C.D., 2001. A geochemical classification for granitic rocks. Journal of Petrology 42, 2033-2048.
Garner, A., McPhie, J., 1999. Partially melted lithic megablocks in the Yardea Dacite, Gawler Range Volcanics, Australia: implications for eruption and emplacement mechanisms. Bulletin of Volcanology 61, 396-410.
Giles, C.W., 1977. Rock units in the Gawler Range Volcanics, Lake Everard area, South Australia. Geological Survey of South Australia, Quarterly Geological Notes 51, 7-16.
Giles, C.W., 1988. Petrogenesis of the Proterozoic Gawler Range Volcanics, South-Australia. Precambrian Research 40-1, 407-427.
Giordano, D., Romano, D.B., Dingwell, D.B., Poe, B., Behrens, H., 2004. The combined effects of water and fluorine on the viscosity of silicic magmas. Geochimica et Cosmochimica Acta 68, 5159-5168.
Giordano, D., Russell, J.K., Dingwell, D.B., 2008. Viscosity of magmatic liquids: A model. Earth and Planetary Science Letters 271, 123-134.

Gray, T.R., Hanley, J.J., Dostal, J., Guillong, M., 2011. Magmatic enrichment of uranium, thorium, and rare earth elements in Late Paleozoic rhyolites of Southern New Brunswick, Canada: evidence from silicate melt inclusions. Economic Geology 106, 127-143.

Green, J.C., Fitz, T.J., 1993. Extensive felsic lavas and rheoignimbrites in the Keweenawan Midcontinent Rift Plateau Volcanics, Minnesota - Petrographic and field recognition. Journal of Volcanology and Geothermal Research 54, 177-196.

Hamilton, M.A., Buchan, K.L., 2010. U-Pb geochronology of the Western Channel Diabase, northwestern Laurentia: Implications for a large 1.59 Ga magmatic province, Laurentia's APWP and paleocontinental reconstructions of Laurentia, Baltica and Gawler craton of southern Australia. Precambrian Research 183, 463-473.

Hand, M., Reid, A., Jagodzinski, L., 2007. Tectonic framework and evolution of the Gawler craton, southern Australia. Economic Geology 102, 1377-1395.

Head, J.W.,III, Coffin, M.F., 1997. Large igneous provinces: a planetary prospective. In: M.F. Coffin, O. Eldholm (Editors), Large igneous provinces: crustal structure, dimensions and external consequences. American Geophysical Union.

Henry, C.D., Price, J.G., Rubin, J.N., Laubach, S.E., 1990. Case-Study of an extensive silicic lava - the Bracks Rhyolite, Trans-Pecos Texas. Journal of Volcanology and Geothermal Research 43, 113-132.

Henry, C.D., Price, J.G., Rubin, J.N., Parker, D.F., Wolff, J.A., Self, S., Franklin, R., Barker, D.S., 1988. Widespread, lava-like silicic volcanic-rocks of Trans-Pecos Texas. Geology 16, 509-512.

Henry, C.D., Wolff, J.A., 1992. Distinguishing strongly rheomorphic tuffs from extensive silicic lavas. Bulletin of Volcanology 54, 171-186.

Holtz, F., Roux, J., Ohlhorst, S., Behrens, H., Schulze, F., 1999. The effects of silica and water on the viscosity of hydrous quartzofeldspathic melts. American Mineralogist 84, 27-36.

Hu, Z.C., Gao, S., 2008. Upper crustal abundances of trace elements: A revision and update. Chemical Geology 253, 205-221.

Kamenetsky, V.S., Danyushevsky, L.V., 2005. Metals in quartz-hosted melt inclusions: Natural facts and experimental artifacts. American Mineralogist 90, 1674-1678.

Keppler, H., 1993. Influence of fluorine on the enrichment of high-field strength trace-elements in granitic-rocks. Contributions to Mineralogy and Petrology 114, 479-488.

Keppler, H., Wyllie, P.J., 1991. Partitioning of Cu, Sn, Mo, W, U, and Th between melt and aqueous fluid in the systems haplogranite-H_2O-HCl and haplogranite-H_2O-HF. Contributions to Mineralogy and Petrology 109, 139-150.

Linnen, R.L., Keppler, H., 2002. Melt composition control of Zr/Hf fractionation in magmatic processes. Geochimica et Cosmochimica Acta 66, 3293-3301.

Lowenstern, J.B., 1995. Applications of silicate melt inclusions to the study of magmatic volatiles. In: J.F.H. Thompson (Editor), Magmas, fluids and ore deposits. Mineralogical Association of Canada Short Course 23, 71-99.

Lowenstern, J.B., Mahood, G.A., 1991. New data on magmatic H_2O contents of pantellerites, with Implications for petrogenesis and eruptive dynamics at Pantelleria. Bulletin of Volcanology 54, 78-83.

Mahoney, M.F., Coffin, M.F., 1997. Large igneous provinces: continental, oceanic and planetary flood volcanism. Geophysical Monograph, 100. American Geophysical Union, 438 pp.

Manley, C.R., 1996. In situ formation of welded tuff-like textures in the carapace of a voluminous silicic lava flow, Owyhee County, SW Idaho. Bulletin of Volcanology 57, 672-686.

Manning, D.A.C., 1981. The effect of fluorine on liquidus phase-relationships in the system Qz-Ab-Or with excess water at 1-Kb. Contributions to Mineralogy and Petrology 76, 206-215.

McPhie, J., DellaPasqua, F., Allen, S.R., Lackie, M.A., 2008. Extreme effusive eruptions: palaeoflow data on an extensive felsic lava in the Mesoproterozoic Gawler Range Volcanics. Journal of Volcanology and Geothermal Research 172, 148-161.

McPhie, J., Doyle, M., Allen, R., 1993. Volcanic textures: a guide to the interpretation of textures in volcanic rocks. University of Tasmania Centre for Ore Deposit and Exploration Studies, Hobart, 198 pp.

McPhie, J., Kamenetsky, V.S., Allen, S., Ehrig, K., Agangi, A., Bath, A., 2011. The fluorine link between a supergiant ore deposit and a silicic large igneous province. Geology 39, 1003-1006.

Métrich, N., Clocchiatti, R., 1989. Melt inclusion investigation of the volatile behavior in historic alkali basaltic magmas of Etna. Bulletin of Volcanology 51, 185-198.

Milner, S.C., Duncan, A.R., Ewart, A., 1992. Quartz latite rheoignimbrite flows of the Etendeka Formation, North-Western Namibia. Bulletin of Volcanology 54, 200-219.

Morrow, N., McPhie, J., 2000. Mingled silicic lavas in the Mesoproterozoic Gawler Range Volcanics, South Australia. Journal of Volcanology and Geothermal Research 96, 1-13.

Münker, C., Pfander, J. A., Weyer, S., Buchl, A., Kleine, T., Mezger, K., 2003. Evolution of planetary cores and the earth-moon system from Nb/Ta systematics. Science 301, 84-87.

Murphy, M.D., Sparks, R.S.J., Barclay, J., Carroll, M.R., Brewer, T.S., 2000. Remobilization of andesite magma by intrusion of mafic magma at the Soufriere Hills Volcano, Montserrat, West Indies. Journal of Petrology 41, 21-42.

Nekvasil, H., 1988. Calculated effect of anorthite component on the crystallization paths of H_2O-undersaturated haplogranitic melts. American Mineralogist 73, 966-981.

Pankhurst, R.J., Leat, P.T., Sruoga, P., Rapela, C.W., Marquez, M., Storey, B.C., Riley, T.R., 1998. The Chon Aike province of Patagonia and related rocks in West Antarctica: A silicic large igneous province. Journal of Volcanology and Geothermal Research 81, 113-136.

Pankhurst, R.J., Rapela, C.R., 1995. Production of Jurassic rhyolite by anatexis of the lower crust of Patagonia. Earth and Planetary Science Letters 134, 23-36.

Pankhurst, R.J., Riley, T.R., Fanning, C.M., Kelley, S.P., 2000. Episodic silicic volcanism in Patagonia and the Antarctic Peninsula: chronology of magmatism associated with the break-up of Gondwana. Journal of Petrology 41, 605-625.

Pankhurst, M.J., Schaefer, B.F., Betts, P.G., Phillips, N. Hand, M., 2011. A Mesoproterozoic continental flood rhyolite province, the Gawler Ranges, Australia: the end member example of the Large Igneous Province clan. Solid Earth 2: 25-33

Parker, D., White, J., 2008. Large-scale silicic alkalic magmatism associated with the Buckhorn Caldera, Trans-Pecos Texas, USA: comparison with Pantelleria, Italy. Bulletin of Volcanology 70, 403-415.

Pearce, J.A., Harris, N.B.W., Tindle, A.G., 1984. Trace element discrimination diagrams for the tectonic interpretation of granitic rocks. Journal of Petrology 25, 956-983.

Peate, D.W., 1997. The Paraná-Etendeka province. In: M.F. Mahoney, M.F. Coffin (Editors), Large igneous provinces: continental, oceanic and planetary flood volcanism. Geophysical Monograph, pp. 217-245.

Pearce, J.A., Harris, N.B.W., Tindle, A.G., 1984. Trace element discrimination diagrams for the tectonic interpretation of granitic rocks. Journal of Petrology 25, 956-983.

Peccerillo, A., Taylor, S.R., 1976. Geochemistry of Eocene calc-alkaline volcanic-rocks from Kastamonu area, northern Turkey. Contributions to Mineralogy and Petrology 58, 63-81.

PIRSA, 2006. Primary Industries and Resources of South Australia Geoscientific GIS Dataset (unpublished).

Qin, Z.W., Lu, F.Q., Anderson, A.T., 1992. Diffusive reequilibration of melt and fluid inclusions. American Mineralogist 77, 565-576.

Rämö, O., Haapala, I., 1995. One hundred years of rapakivi granite. Mineralogy and Petrology 52, 129-185.

Riley, T.R., Leat, P.T., Pankhurst, R.J., Harris, C., 2001. Origins of large volume rhyolitic volcanism in the Antarctic Peninsula and Patagonia by crustal melting. Journal of Petrology 42, 1043-1065.

Romano, C., Poe, B., Mincione, V., Hess, K.U., Dingwell, D.B., 2001. The viscosities of dry and hydrous $XAlSi_3O_8$ (X = Li, Na, K, Ca-0.5, Mg-0.5) melts. Chemical Geology 174, 115-132.

Rubatto, D., Hermann, J., 2007. Experimental zircon/melt and zircon/garnet trace element partitioning and implications for the geochronology of crustal rocks. Chemical Geology 241, 38-61.

Skirrow, R.G., Bastrakov, E., Davidson, G.J., Raymond, O., Heithersay, P., 2002. Geological framework, distribution and controls of Fe-oxide Cu- Au deposits in the Gawler craton. Part II. Alteration and mineralization. In: T.M. Porter (Editor), Hydrothermal iron oxide copper-gold and related deposits. Porter GeoConsultancy, Adelaide, pp. 33-47.

Skirrow, R.G., Bastrakov, E.N., Baroncii, K., Fraser, G.L., Creaser, R.A., Fanning, C.M., Raymond, O.L., Davidson, G.J., 2007. Timing of iron oxide Cu-Au-(U) hydrothermal activity and Nd isotope constraints on metal sources in the Gawler craton, South Australia. Economic Geology 102, 1441-1470.

Stewart, K.P., 1994. High temperature silicic volcanism and the role of mantle magmas in Proterozoic crustal growth: the Gawler Range Volcanic Province, University of Adelaide, Adelaide.

Sun, S.S., McDonough, W.F., 1989. Chemical and isotopic systematics of oceanic basalts: implications for mantle composition and processes. In: A.D. Saunders, Norry, M. J. (Editor), Magmatism in the Ocean Basins. Geological Society of London Special Publication 42, 313-345.

Thomas, J.B., Bodnar, R.J., Shimizu, N., Sinha, A.K., 2002. Determination of zircon/melt trace element partition coefficients from SIMS analysis of melt inclusions in zircon. Geochimica et Cosmochimica Acta 66, 2887-2901.

Twist, D., French, B.M., 1983. Voluminous acid volcanism in the Busheveld Complex: a review of the Rooiberg Felsite. Bulletin Volcanologique 46, 225-242.

Walker, G.P.L., 1973. Lengths of lava flows. Philosophical Transactions of the Royal Society of London A 274, 107-118.

Walker, G.P.L., 1980. Low aspect ratio ignimbrites. Nature 283, 286-287.

Walker, G.P.L., 1983. Ignimbrite types and ignimbrite problems. Journal of Volcanology and Geothermal Research 17, 65-88.

Watson, E.B., Harrison, T.M., 1983. Zircon saturation revisited: temperature and composition effects in a variety of crustal magma types. Earth and Planetary Science Letters 64, 295-304.

Webster, J.D., 1990. Partitioning of F between H_2O and CO_2 fluids and topaz rhyolite melt - Implications for mineralizing magmatic-hydrothermal fluids in F-rich granitic systems. Contributions to Mineralogy and Petrology 104, 424-438.

Wedepohl, K.H., 1995. The composition of the continental crust. Geochimica et Cosmochimica Acta, 59: 1217-1232.

Whalen, J.B., Currie, K.L., Chappell, B.W., 1987. A-type granites - Geochemical characteristics, discrimination and petrogenesis. Contributions to Mineralogy and Petrology 95, 407-419.

White, J.C., Holt, G.S., Parker, D.F., Ren, M.H., 2003. Trace-element partitioning between alkali feldspar and peralkalic quartz trachyte to rhyolite magma. Part I: Systematics of trace-element partitioning. American Mineralogist 88, 316-329.

Wilson, C.J.N., Houghton, B.F., Kampt, P.J.J., McWilliamst, M.O., 1995. An exceptionally widespread ignimbrite with implications for pyroclastic flow emplacement. Nature 378, 605-607.

Wolff, J.A., Wright, J.V., 1981. Rheomorphism of welded tuffs. Journal of Volcanology and Geothermal Research 10, 13-34.

Wright, J.V., Smith, A.L., Self, S., 1980. A working terminology of pyroclastic deposits. Journal of Volcanology and Geothermal Research 8, 315-336.

Fig. 1. Simplified geological map of the Gawler Range Volcanics and Hiltaba Suite granite (**a**), Chitanilga Volcanic Complex at Kokatha (**b**) and Glyde Hill Volcanic Complex at Lake Everard (**c**). Inset indicates the Gawler Craton and Proterozoic units in Australia. After Blissett (1975); Blissett et al. (1993); Giles (1977); Allen and McPhie (2002); Hand et al. (2007). Grid: GDA94.

Fig. 2. Simplified logs of the lower Gawler Range Volcanics: the Glyde Hill and Chitanilga Volcanic Complexes.

Fig. 3. Textures of the lower GRV: Glyde Hill Volcanic Complex, Lake Everard. **a** Wheepool Rhyolite (GH23, GR 0517647-6488394, polished block). Phenocrysts are an- to subhedral, but largely unbroken; inset: accessory minerals (back-scattered electron image, BSE). **b** Mangaroongah Dacite (GH21, GR 0515440-6484867, polished block); inset: Ca-pyroxene, apatite and unmixed Fe-Ti oxide (BSE). **c** Folded flow bands in the Baldry Rhyolite. Arrow indicates axis plunge (GR 0509831-6501976). **d** Flow bands in the Baldry Rhyolite shown in a section perpendicular to flow direction. Concentric structures (dashed lines) represent intersected culmination of non-cylindrical folds. **e** Amygdaloidal autobreccia clast, Mangaroongah Dacite. (GR 0486138-6490540). **f** Autobreccia domain in the Mangaroongah Dacite. Dashed line indicates lobate clast (GR 0486261-6500298). **g** Waurea Pyroclastics (sample GH95, 0515405-6501456, polished block); inset: bubble-wall shard matrix (BSE). **h** Moonamby Dyke Suite (sample GH92, GR 0486550-6489826, polished block); inset: quartz phenocrysts in microcrystalline groundmass (plane polarised transmitted light). GR: Grid reference (GDA94).

Fig. 4. Felsic igneous enclaves. **a** Gradational contact between an igneous enclave (granite, left) and the host volcanic unit (Whyeela Dacite, right) (GR 0523705-6495238). **b** Anhedral mm-scale K-feldspar and quartz in fine grained groundmass (sample GH29, GR 0 524305–6495515, thick section scan). **c** Anhedral K-feldspar crystal surrounded by a fine grained quartz-K-feldspar granophyric rim (sample GH32, GR 0523705-6495238, parallel polarised transmitted light). **d** Aggregate of quartz and fine grained epidote (sample GH32, parallel polarised transmitted light). GR: Grid reference (GDA94).

Fig. 5. Textures of the lower GRV: Chitanilga Volcanic Complex, Kokatha. **a** Eutaxitic-textured ignimbrite, Lake Gairdner Rhyolite (sample GH51, GR 0524029-6542642, polished block); inset: bubble-wall shard matrix (BSE). **b** Crystal fragments (some arrowed) suggest explosive eruption mechanism, even if the matrix does not preserve evidence of fragmental texture, Lake Gairdner Rhyolite (sample GH51, GR 0524029-6542642, scanned thick section). **c** Open asymmetric folds (GR 0524988-6541028), **d** Ptygmatic folds (GR 0525008-6541038), and **e** isoclinal fold showing parallelism between elongation lineation and hinge line (0525170-6541134), Rhyolite-dacite (Mi5). **f** Diagrammatic log, and stereographic plot of fold limbs, elongation lineation and fold axes in the Rhyolite-dacite (Mi5). Deformation structures indicate a northwest-directed flow. GR: Grid reference (GDA94).

Fig. 6. Melt inclusions in the lower GRV. **a** and **b** Glass-bearing, subhedral negative crystal-shaped inclusions (Waurea Pyroclastics, sample GH95 and 13, respectively). **c** Subhedral negative crystal-shaped, crystalline melt inclusions (Moonamby Dyke Suite, sample GH15). **d** Multiple melt inclusions trapped at various growth stages of the quartz host (Waurea Pyroclastics, sample GH95, unheated). **e** Homogenised melt inclusion showing round and slightly irregular margins (Wheepool Rhyolite, sample GH23, heated to 1000°C). **f** Unsuccessful homogenisation attempt (Waurea Pyroclastics, sample GH13, heated to 1050°C). All images are in plain polarised transmitted light.

Fig. 7. Melt inclusion (EPMA) and whole-rock (XRF) major element compositions. Data recalculated to 100% anhydrous and plotted as wt.%. [1] Whole-rock data, large

symbols: this study, small symbols: Ferris (2001); Stewart (1994); PIRSA (2006). [2] Melt inclusion data, lower GRV: this study, upper GRV: McPhie et al. (2011). Low, mid, high, and ultra-K fields after Peccerillo and Taylor (1976).

Fig. 8. Melt inclusion (LA-ICP-MS, EPMA) and whole-rock (ICP-MS, XRF) trace element compositions. Data plotted as ppm, except SiO_2 recalculated to 100% anhydrous and plotted as wt.%. [1] Whole-rock data, large symbols: this study, small symbols: Ferris (2001); Stewart (1994); PIRSA (2006). [2] Melt inclusion data, lower GRV: this study, upper GRV: McPhie et al. (2011). Chondrite and primitive mantle values from Sun and McDonough (1989) and Münker et al. (2003).

Fig. 9. Primitive mantle-normalised whole-rock and melt inclusion compositions of the lower GRV. Melt inclusions: Wheepool Rhyolite average (n = 13). Normalising values after Sun and McDonough (1989).

Fig. 10. Comparison of the GRV with other SLIP and large felsic units worldwide. Lower GRV (this study); upper GRV (Stewart, 1994), Chon-Aike Province, Patagonia (Pankhurst and Rapela, 1995); Mapple and Poster Formations, Antarctic Peninsula (Riley, 2001); Sierra Madre Occidental, Mexico (Cameron, 1980); Whitsunday Province, Queensland (average values, Bryan et al., 2000); SNP-Yellowstone: Snake River Plain and Yellowstone, western USA (compiled by Christiansen and McCurry, 2008); Etendeka, Namibia (Ewart et al., 2004). Modified iron number (Fe* number = $FeO_{tot}/(FeO_{tot} + MgO)$) after Frost et al. (2001). UCC: upper continental crust (Hu and Gao, 2008). Nb vs 10000·Ga/Al after Whalen et al. (1987). Nb vs Y diagram after Pearce (1984), WPG: within-plate granite, VAG: volcanic arc granite, COLG: collisional granite, ORG: orogenic granite.

Fig 11. Modelling of crystallisation of andesite (sample GH39) compared with melting of granite (sample GH37). Both equilibrium and disequilibrium processes are compared. Numbers indicate fraction of solid (0.2 - 1). Equilibrium processes appear inadequate to explain wide compositional variations. Crystal-melt distribution coefficients: Ba 2.1, Sr 1.36, Nb 0.2, Th 0.2.

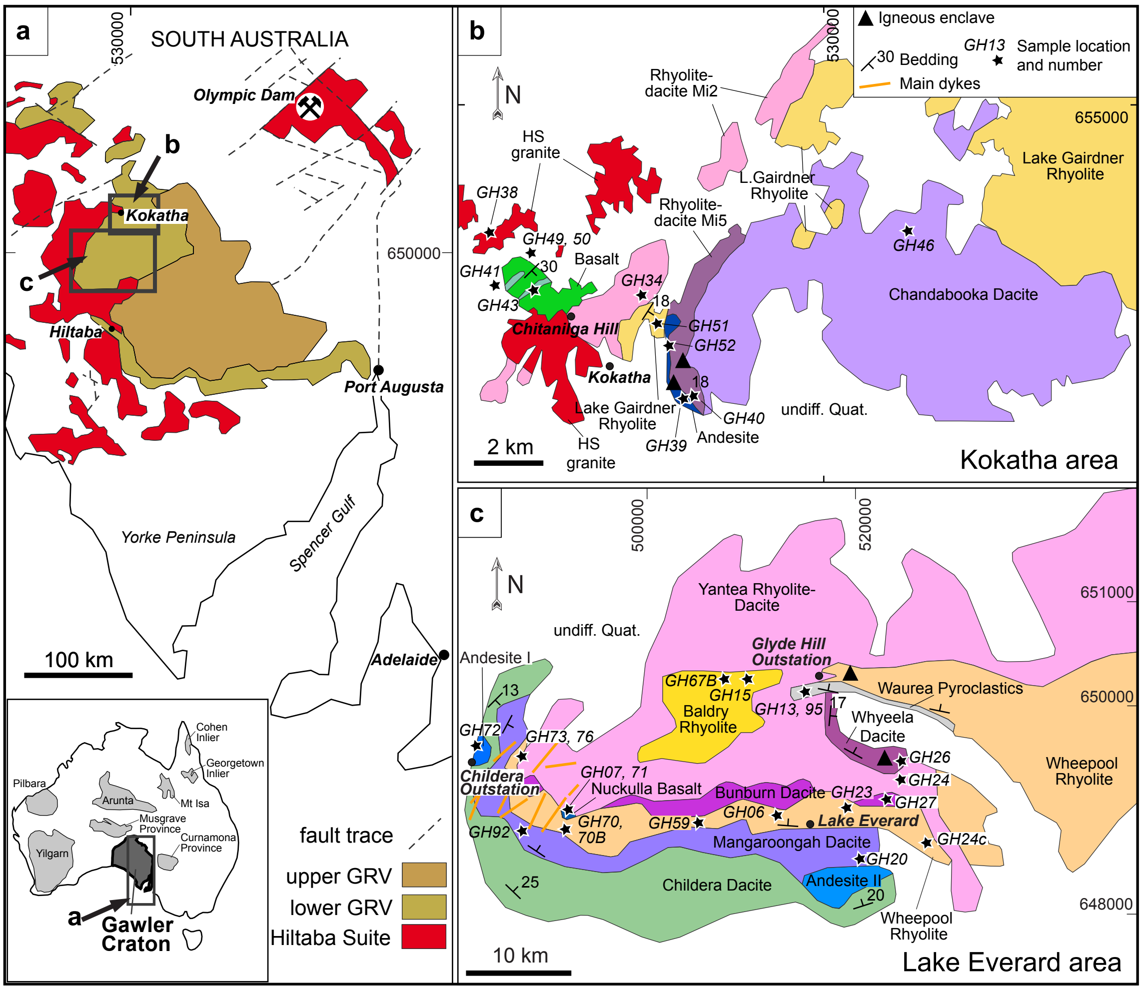
a
SOUTH AUSTRALIA
530000
Olympic Dam
b
Kokatha
c
Hiltaba
650000
Port Augusta
Yorke Peninsula
Spencer Gulf
Adelaide
100 km
fault trace
upper GRV
lower GRV
Hiltaba Suite
Pilbara
Cohen Inlier
Georgetown Inlier
Arunta
Mt Isa
Musgrave Province
Curnamona Province
Yilgarn
a
Gawler Craton
b
N
Igneous enclave
30 Bedding
GH13 Sample location and number
Main dykes
530000
655000
Rhyolite-dacite Mi2
HS granite
GH38
L.Gairdner Rhyolite
Lake Gairdner Rhyolite
Rhyolite-dacite Mi5
GH46
GH49, 50
Basalt
GH41
30
GH34
GH43
18
Chandabooka Dacite
GH51
Chitanilga Hill
GH52
Kokatha
18
Lake Gairdner Rhyolite
GH40
undiff. Quat.
Andesite
2 km
HS granite
GH39
Kokatha area
c
500000
520000
N
Yantea Rhyolite-Dacite
651000
undiff. Quat.
Glyde Hill Outstation
Andesite I
GH67B
GH15
Waurea Pyroclastics
650000
13
Baldry Rhyolite
GH13, 95
17
GH72
Whyeela Dacite
GH73, 76
GH26
Wheepool Rhyolite
Childera Outstation
GH07, 71
GH24
Nuckulla Basalt
Bunburn Dacite
GH23
GH27
GH06
GH70, 70B
GH59
Lake Everard
GH92
GH24c
Mangaroongah Dacite
GH20
25
Childera Dacite
Andesite II
20
648000
Wheepool Rhyolite
10 km
Lake Everard area

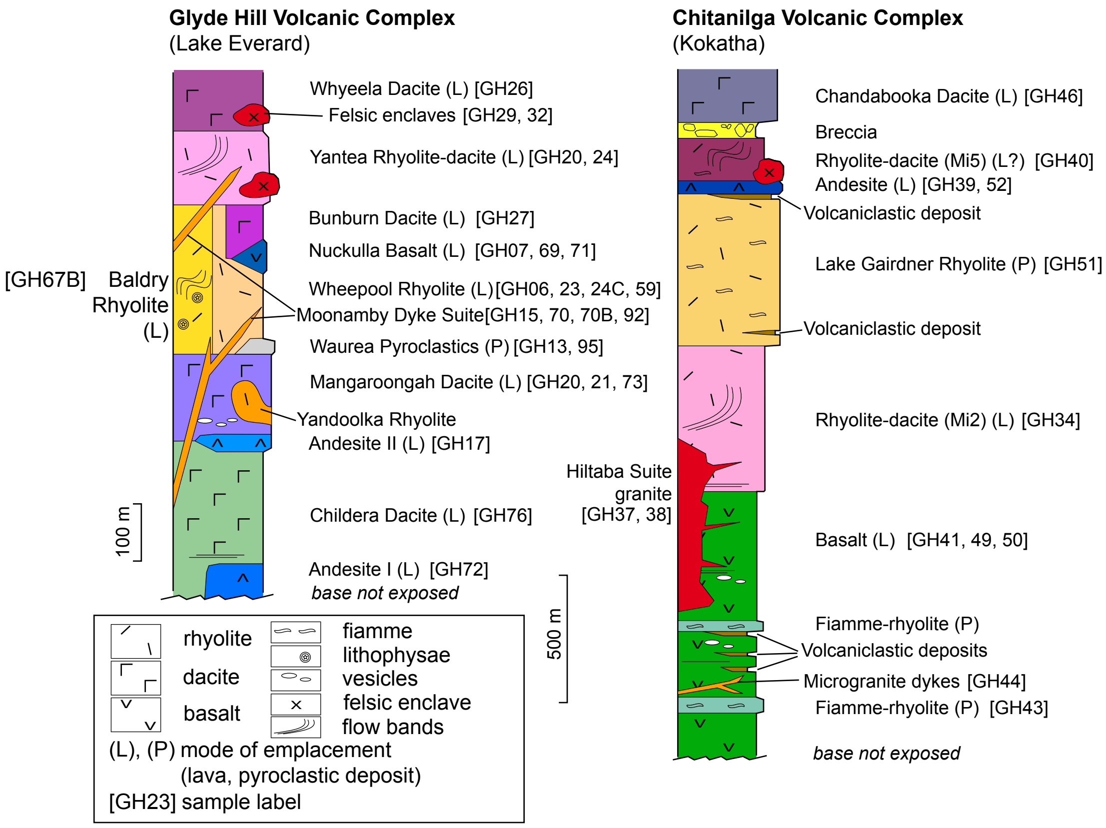

Glyde Hill Volcanic Complex
(Lake Everard)
Whyeela Dacite (L) [GH26]
Felsic enclaves [GH29, 32]
Yantea Rhyolite-dacite (L) [GH20, 24]
Bunburn Dacite (L) [GH27]
Nuckulla Basalt (L) [GH07, 69, 71]
[GH67B] Baldry Rhyolite (L)
Wheepool Rhyolite (L) [GH06, 23, 24C, 59]
Moonamby Dyke Suite [GH15, 70, 70B, 92]
Waurea Pyroclastics (P) [GH13, 95]
Mangaroongah Dacite (L) [GH20, 21, 73]
Yandoolka Rhyolite
Andesite II (L) [GH17]
100 m
Childera Dacite (L) [GH76]
Andesite I (L) [GH72]
base not exposed
rhyolite
dacite
basalt
fiamme
lithophysae
vesicles
felsic enclave
flow bands
(L), (P) mode of emplacement
(lava, pyroclastic deposit)
[GH23] sample label
500 m
Chitanilga Volcanic Complex
(Kokatha)
Chandabooka Dacite (L) [GH46]
Breccia
Rhyolite-dacite (Mi5) (L?) [GH40]
Andesite (L) [GH39, 52]
Volcaniclastic deposit
Lake Gairdner Rhyolite (P) [GH51]
Volcaniclastic deposit
Rhyolite-dacite (Mi2) (L) [GH34]
Hiltaba Suite granite [GH37, 38]
Basalt (L) [GH41, 49, 50]
Fiamme-rhyolite (P)
Volcaniclastic deposits
Microgranite dykes [GH44]
Fiamme-rhyolite (P) [GH43]
base not exposed

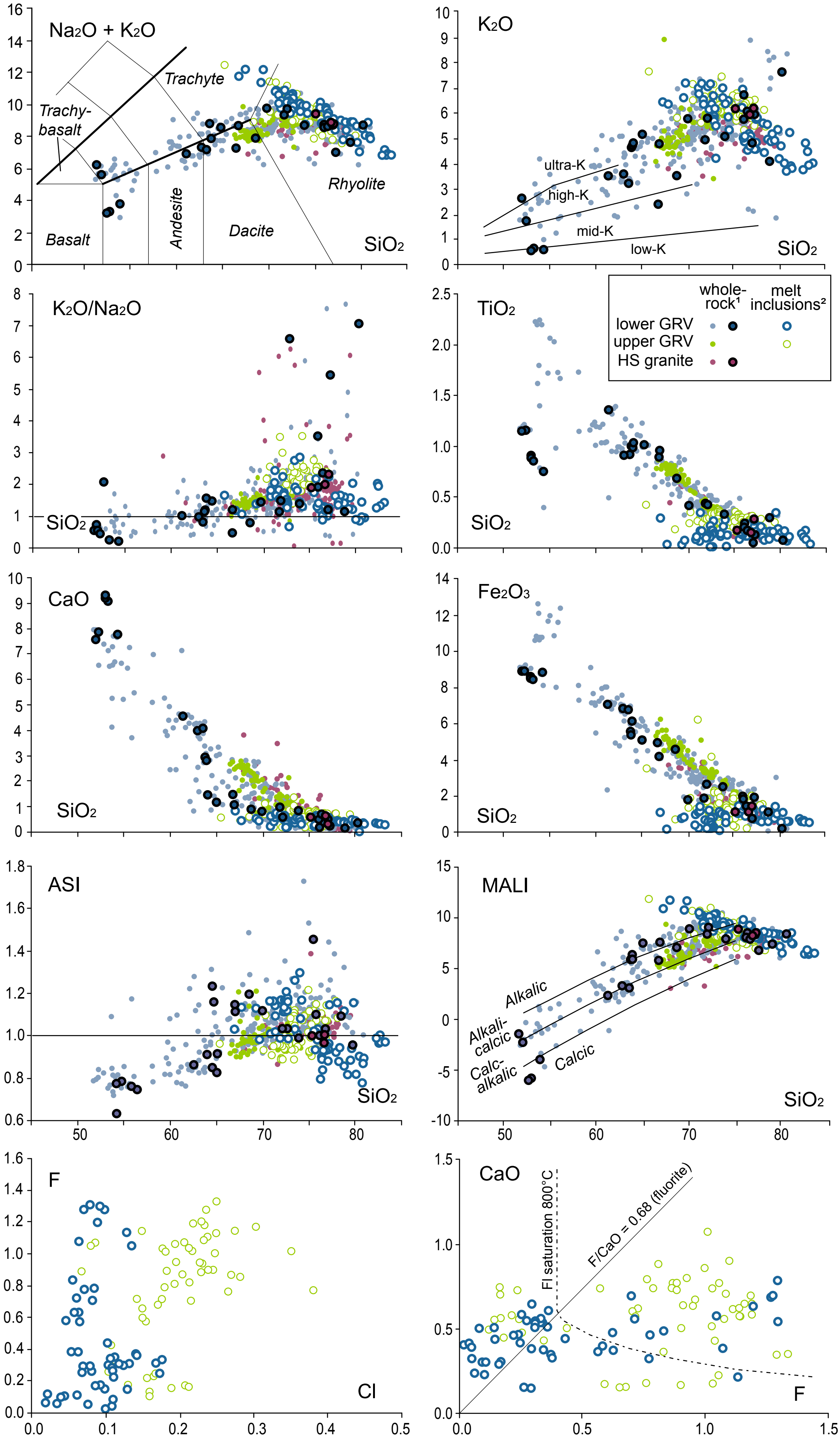

Na2O + K2O
Trachyte
Trachy-basalt
Basalt
Andesite
Dacite
Rhyolite
SiO2
K2O
ultra-K
high-K
mid-K
low-K
K2O/Na2O
TiO2
whole-rock¹
melt inclusions²
lower GRV
upper GRV
HS granite
CaO
Fe2O3
ASI
MALI
Alkalic
Alkali-calcic
Calc-alkalic
Calcic
F
Cl
Fl saturation 800°C
F/CaO = 0.68 (fluorite)

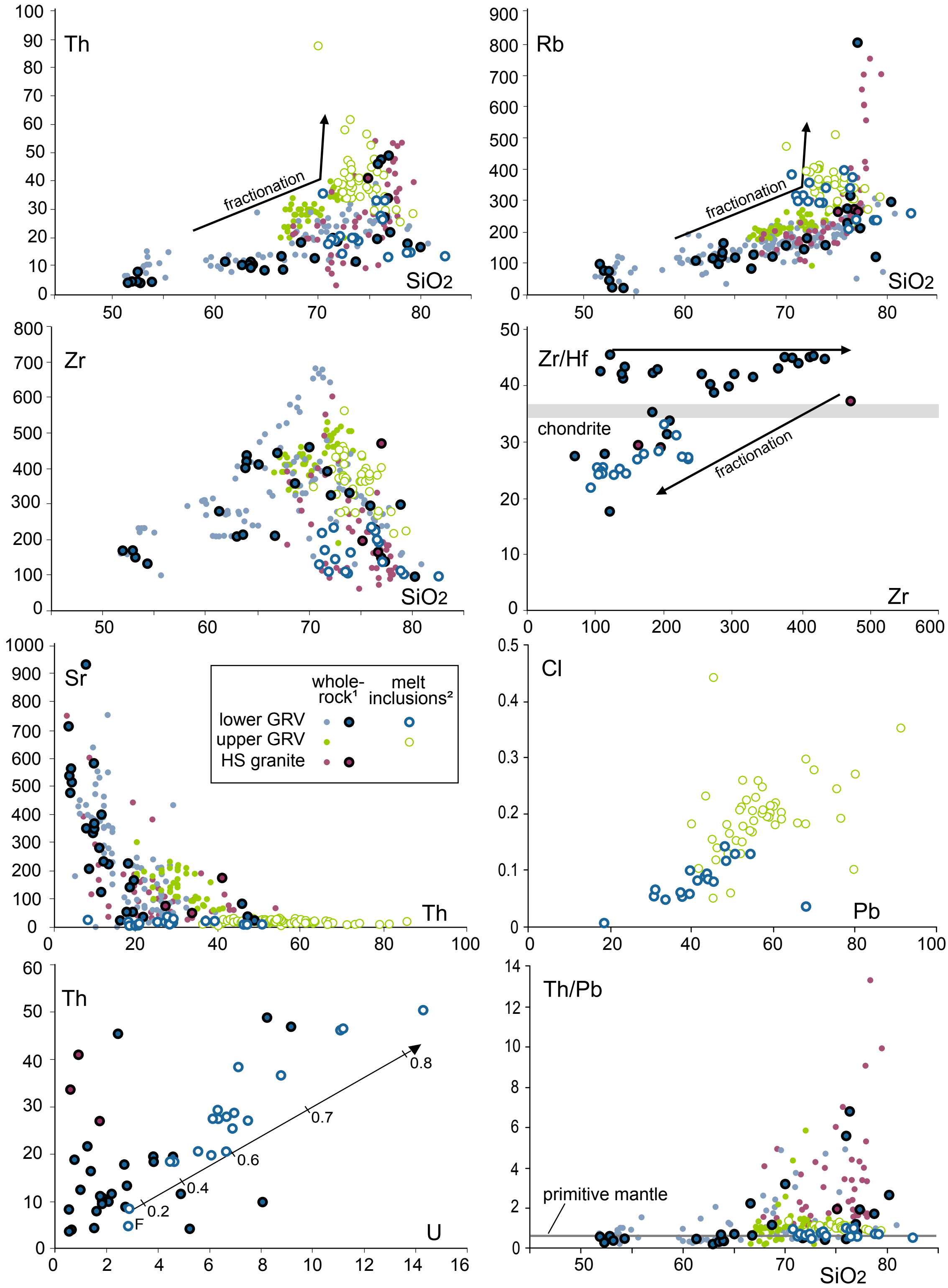

Th
fractionation
SiO2
Rb
fractionation
SiO2
Zr
SiO2
Zr/Hf
chondrite
fractionation
Zr
Sr
whole-rock¹
melt inclusions²
lower GRV
upper GRV
HS granite
Th
Cl
Pb
Th
0.2
0.4
0.6
0.7
0.8
F
U
Th/Pb
primitive mantle
SiO2

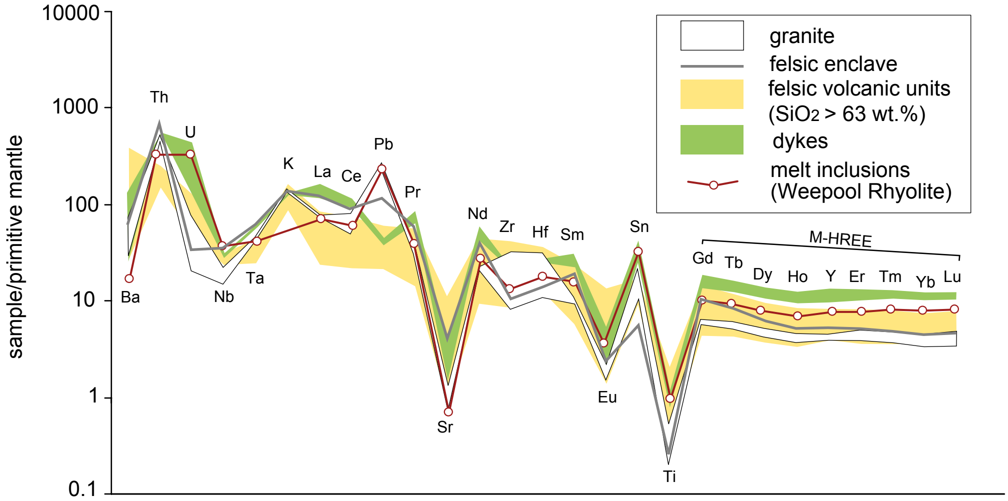

10000
1000
100
10
1
0.1
sample/primitive mantle
Ba
Th
U
Nb
Ta
K
La
Ce
Pb
Pr
Sr
Nd
Zr
Hf
Sm
Eu
Sn
Ti
M-HREE
Gd
Tb
Dy
Ho
Y
Er
Tm
Yb
Lu
granite
felsic enclave
felsic volcanic units
(SiO2 > 63 wt.%)
dykes
melt inclusions
(Weepool Rhyolite)

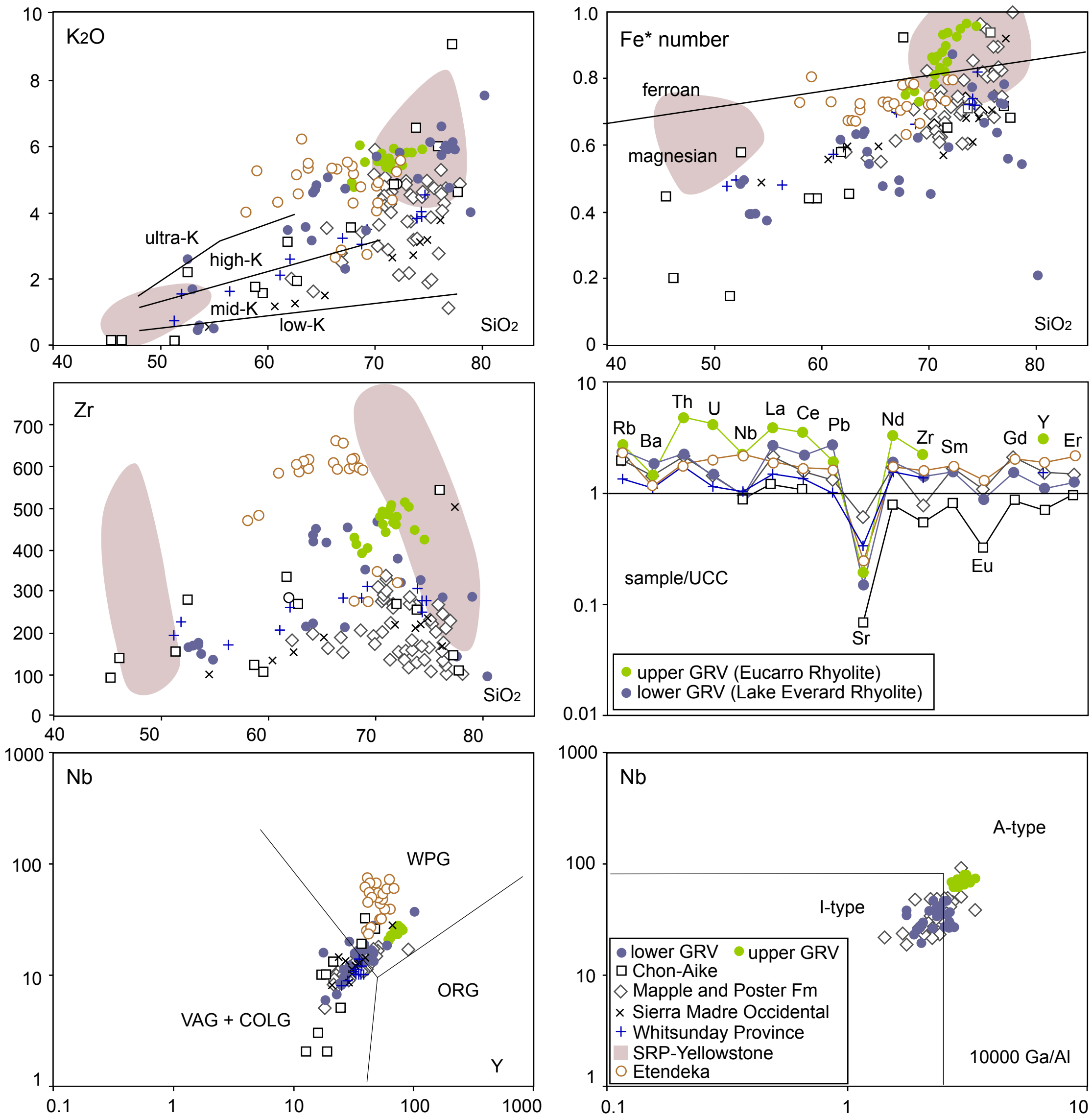

K2O
ultra-K
high-K
mid-K
low-K
SiO2
Fe* number
ferroan
magnesian
SiO2
Zr
SiO2
Rb
Ba
Th
U
Nb
La
Ce
Pb
Nd
Zr
Sm
Gd
Y
Er
Sr
Eu
sample/UCC
upper GRV (Eucarro Rhyolite)
lower GRV (Lake Everard Rhyolite)
Nb
WPG
ORG
VAG + COLG
Y
Nb
A-type
I-type
lower GRV
upper GRV
Chon-Aike
Mapple and Poster Fm
Sierra Madre Occidental
Whitsunday Province
SRP-Yellowstone
Etendeka
10000 Ga/Al

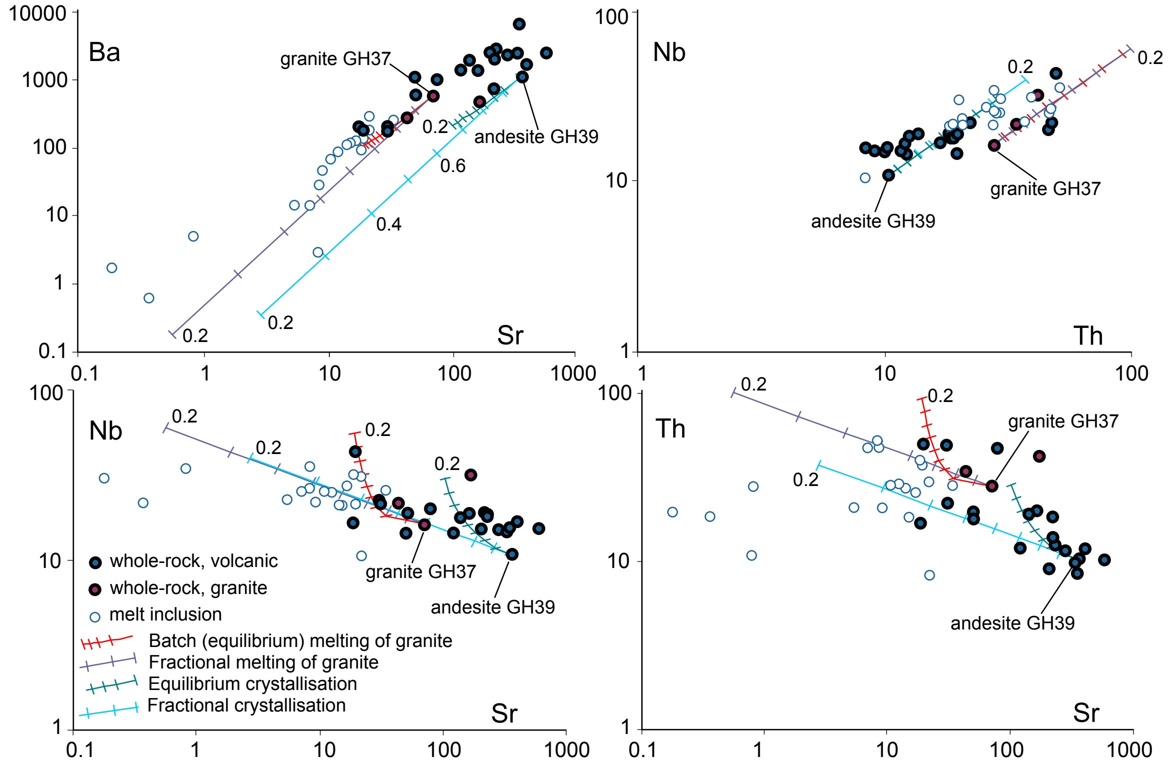

Ba
granite GH37
andesite GH39
0.2
0.6
0.4
0.2
0.2
Sr
Nb
0.2
0.2
granite GH37
andesite GH39
Th
Nb
0.2
0.2
0.2
0.2
granite GH37
andesite GH39
Sr
whole-rock, volcanic
whole-rock, granite
melt inclusion
Batch (equilibrium) melting of granite
Fractional melting of granite
Equilibrium crystallisation
Fractional crystallisation
Th
0.2
0.2
0.2
granite GH37
andesite GH39
Sr

Table 1. Characteristics of some felsic and bimodal large igneous provinces

Volcanic province	Primary emplacement mechanism	Volume (km3)	Age (Ma)	Extrusion rate (km3 /year)	Reference	Magma temperature	Paragenesis of felsic rocks
Gawler Range Volcanics, Australia	lava	25000	1591–1592	0.0125	Blissett et al., 1993; Fanning, 1988	900-1100°C	Qtz, fls, ±CPx, Zrn, Ap, Fe-Ti ox, ±Fl
Keweenawan Midcontinent Rift Plateau, USA	lava, ignimbrite	/	1100		Green and Fitz, 1993	1000-1100°C	Pl, Kfs, ±Qtz, ±Aug, Mag, Zrn, Ap, ±Fl
Chon-Aike, Patagonia and Anctartic Peninsula	ignimbrite	230000	188–153	0.0066	Pankhurst et al., 1998; 2000	/	Qtz, Pl, Kfs, Biot, Am, Mag, Il, Ap
Whitsunday, Australia	ignimbrite	2200000	132–95	0.0595	Bryan et al., 2000	/	Qtz, Pl, Cpx, Biot, Am, Ti-Mag
Sierra Madre Occidental, Mexico	ignimbrite	390000	38–20	0.0217	Cameron et al., 1980; Ferrari et al., 2002; Bryan et al., 2008	750-900°C	Pl, Opx, Cpx, Am, Mag, Il
Snake River Plain-Yellowstone	lava, ignimbrite	/	Neogene		Christiansen and McCurry, 2008	830-1050	Pl, Qtz, Fe-Ti ox, CPx, ±Am, ±Biot
Paraná-Etendeka province (silicic component)	lava	/	132±1-130		Marsh et al., 2001	≥1000°C	Pl, CPx, Fe-Ti ox, ±Opx, Ap

Table 2. Volcanic textures and emplacement mechanisms of selected felsic units in the lower GRV

Unit	Area* (km2)	Volume* (km3)	Aspect ratio**	Texture	Groundmass/ matrix	Phenocrysts/ crystals	Breccia domains	Flow deformation	Enclaves, xenocrysts	Emplacement mechanism interpretation
Childera Dacite	267	81	61	coherent	microcrystalline	sub- to an-hedral	angular clasts and thin breccia layers	flow bands, lineation	no	lava flow
Mangaroongah Dacite	136	27	66	coherent	microcrystalline	eu- to sub-hedral or anhedral sieve-textured, glomerocrysts	angular or lobed amygdaloidal clasts and thin breccia layers	autobreccia, deformed vesicles	no	lava flow
Wheepool Rhyolite	511	153	85	coherent	microcrystalline, locally flow-banded	anhedral	lobed clasts (autobreccia)	flow bands, autobreccia	no	lava flow
Baldry Rhyolite	94	5	219	coherent	microcrystalline, µm-scale layering	eu- to sub-hedral	angular ±jigsaw-fit clasts	folded flow bands, lineation	no	lava flow
Bunburn Dacite	67	7	93	coherent	microcrystalline	sub- to eu-hedral	no	no	no	lava flow(?)
Yantea Rhyolite-dacite	1123	168	252	coherent	microcrystalline, locally fiamme-bearing at base	an- to eu-hedral	angular clasts	flow bands, autobreccia	Qtz-fls enclaves	lava flow
Rhyolite-dacite (Mi2)	11	7	6	coherent	microcrystalline	anhedral	no	folded flow bands, lineation, elongate vesicles	rare lithic fragments	lava flow
Lake Gairdner Rhyolite	120	48	31	clastic	eutaxitic, glass shards, fiamme-bearing	anhedral, fractured	no	no	rare lithic fragments	ignimbrite
Rhyolite-dacite (Mi5)	4	1	12	coherent	locally fiamme-bearing, layered	eu- to sub-hedral	no	folded flow bands, lineation	Qtz-fls enclaves	lava flow(?)
Chandabooka Dacite	77	23	33	coherent	microcrystalline	eu- to an-hedral	angular clasts at base	flow bands	no	lava flow

*Outcrop area and volume are calculated by interpolation of outcrops and represent minimum estimates

** Aspect ratio: diameter of circle of equivalent area/average thickness

Table 3. Textural and compositional characteristics of the lower GRV

Rock type	Rhyolite lavas	Pyroclastic deposits	Dacite lavas	Basalt, basaltic andesite	Rhyolite dykes	Granite
Texture	porphyritic	massive-eutaxitic	porphyritic	sparsely porphyritic, ±amygdaloidal	porphyritic	equigranular-seriate
Max grain size	5 mm	2 mm	5 mm	1 mm	3 cm	10 mm
Phenocrysts/ crystals	Ab, Kfs, ±Qtz	Qtz, Kfs, Ab	Ab, Kfs, ±Cpx, ±xenocrystic Qtz	Cpx, ±(altered) Ol?	Qtz, Ab, Kfs	Qtz, Kfs, Ab, Bt
Groundmass	Qtz, Kfs, Ab	Qtz, Kfs	Ab, Kfs, Qtz	Pl, Cpx	Qtz, Ab, Kfs	
Accessory and [alteration] minerals	Ap, Zrn, Fe-Ti ox, Ti ox, ±REE-F-Cb, ±Mnz	Zrn, Fe(-Ti) ox, Fl, [Ttn]	Fe ox, Ap, Zrn, Ti ox, ±REE-F-Cb, [±Ep, ±Chl]	Fe ox	Fe ox, Ti ox, Fl, Ap, Zrn, REE-F-Cb	Fe ox, Fl, Zrn, Ap
Groundmass/matrix texture	microcrystalline (≤20 μm)	vitriclastic (≤500 μm)	microcrystalline-micropoikilitic (≤50 μm)	microcrystalline (≤100 μm)	microcrystalline (≤100 μm), ±poikilitic Qtz	-
Phenocryst abundance/ crystal proportion	≤10%	<20%	≤10%	<5 %	20-30%	-
Igneous enclaves	x		x			

Abbreviations: Ab albite, Ap apatite, Bt biotite, Cb carbonate, Fl fluorite, Kfs K-feldspar, Mag magnetite, Mnz monazite, Ol olivine, ox oxide, Cpx clinopyroxene, Qtz quartz, Ttn titanite, Zrn zircon.

Table 4. Whole-rock compositions

Sample		GH06 (MI)*	GH13 (MI)*	GH27	GH67B	GH34*	GH40	GH43	GH46	GH51**	GH15 (MI)*	GH70*	GH44*	GH07	GH17	GH20	GH24	GH26	GH69	GH71	GH72	GH73	GH76	GH39	GH41	GH49	GH50	GH52	GH37**	GH38	GH32**
Unit	detection li	WR	WP	BD	BR	RDMi2	RDMi5	FR	CD	LGR	MDS	MDS	MGD	NB	AII	MD	YRD	WD	B	NB	AI	MD	ChD	A	B	B	B	A	HS	HS	FE
Volcanic complex		GHVC	GHVC	GHVC	GHVC	CVC	CVC	CVC	CVC	CVC	GHVC	GHVC	CVC	GHVC	GHVC	GHVC	GHVC	GHVC	CVC	GHVC	GHVC	GHVC	GHVC	CVC	CVC	CVC	CVC	CVC			
SiO2 (wt.%)		78.16	74.85	68.57	79.66	71.65	73.2	71	67.11	75.67	75.6	75.16	76.44	52.48	62.82	61.74	65.18	62.63	51.03	50.9	60.07	62.36	65.1	62.92	52.28	52.12	53.2	62.35	76.25	76.26	74.66
TiO2		0.29	0.12	0.4	0.08	0.42	0.32	0.43	0.66	0.19	0.16	0.23	0.04	0.84	0.97	0.96	0.93	0.98	1.13	1.12	1.32	1.01	0.87	0.9	0.89	0.87	0.73	0.9	0.15	0.28	0.17
Al2O3		11.23	11.93	15.37	9.99	13.87	12.66	14.45	14.34	12.1	11.88	12.19	12.66	16.02	14.5	14.5	14.51	14.23	16.95	16.86	14.1	14.92	13.79	13.96	15.87	15.66	14.37	14.22	12.12	11.55	12.95
Fe2O3		1.24	2.1	1.94	0.19	2.98	2.8	2.03	5.08	2.2	1.56	2.03	0.81	9.41	5.95	6.1	4.61	5.5	9.9	9.84	7.83	6.73	5.44	7.58	9.63	9.57	9.81	7.7	1.21	1.6	1.25
MnO		0.03	0.03	0.08	0.01	0.03	0.07	0.06	0.14	0.11	0.06	0.01	0.02	0.14	0.16	0.14	0.11	0.15	0.15	0.14	0.2	0.12	0.18	0.12	0.14	0.14	0.17	0.13	0.02	0.03	0.05
MgO		0.53	0.83	1.17	0.36	0.21	0.41	0.69	1.55	0.24	0.44	0.34	0.16	7.17	2.14	1.69	2.29	2.98	5.3	5.01	2.44	2.82	3.17	2.15	7.35	7.48	8.25	2.31	0.23	0.22	0.31
CaO		0.11	0.17	0.77	0.31	0.55	0.81	0.93	0.83	0.46	0.69	0.14	0.42	8.95	2.72	2.79	0.99	1.07	7.41	7.6	4.41	1.4	1.4	4	9.05	9.11	7.55	3.92	0.6	0.27	0.54
Na2O		3.47	1.04	3.85	1.06	3.84	3.64	4.33	4.3	1.87	2.54	2.93	3.95	2.65	3.93	3.95	3.79	3.32	3.5	3.79	3.35	2.98	4.77	3.9	2.6	2.62	3.09	3.66	2.91	2.61	3.22
K2O		4	5.68	5.61	7.5	5.73	4.96	4.82	3.36	6.61	5.95	5.63	4.71	0.58	4.6	4.45	4.59	4.9	2.54	1.64	3.37	4.64	2.28	3.14	0.53	0.51	0.55	3.5	5.83	6.06	6.08
P2O5		0.04	0.02	0.13	0.02	0.06	0.05	0.04	0.2	0.02	0.02	0.05	0.03	0.29	0.39	0.37	0.34	0.39	0.25	0.25	0.77	0.38	0.49	0.22	0.31	0.31	0.23	0.21	0.03	0.04	0.02
BaO		0.12	0.03	0.46	<0.03	0.36	0.25	0.24	0.34	0.19	0.07	0.19	0.03	0.04	0.42	0.39	0.44	1.09	0.1	0.07	0.29	0.41	0.12	0.19	0.09	0.08	0.07	0.19	0.1	0.07	0.1
loss(inc S-)		0.97	2.81	2.09	0.94	0.36	0.43	0.61	1.95	0.44	1.37	1	0.71	1.27	1.32	3	1.91	3.22	2.1	2.66	2.04	2.04	2.25	0.7	1.2	1.16	1.73	1.21	0.5	0.56	0.82
Total		100.19	99.62	100.44	100.12	100.06	99.6	99.63	99.87	100.1	100.34	99.9	99.98	99.85	99.93	100.08	99.69	100.46	100.36	99.87	100.19	99.81	99.87	99.78	99.95	99.63	99.75	100.29	99.95	99.54	100.17
S		<0.01	<0.01	0.02	0.01	<0.01	<0.01	<0.01	0.01	<0.01	<0.01	0.01	0.01	<0.01	<0.01	<0.01	<0.01	0.13	<0.01	<0.01	<0.01	<0.01	<0.01	<0.01	<0.01	<0.01	<0.01	<0.01	<0.01	<0.01	<0.01
Li (ppm)	0.016	10	14.5	12.3	5.1	4.1	8.1	12.1	21	5.7	13	7.6	30	16.2	18.8	17.6	42.9	28.5	23	42.2	23.1	32.2	31.9	17.4	25	25	18.1	21.2	10.7	10.4	5.2
Be	0.008	2	2.41	1.95	1.59	3.13	2.78	2.72	3.37	2.3	4.35	3.64	6.26	0.98	2.3	2.27	2.57	2.08	1.2	0.97	2.58	2.62	3.08	2.03	1.11	1.48	0.97	1.78	3.27	2.29	3.72
Sc	0.038	4.6	3.3	6.7	2.2	6.2	6.8	7	10.7	6.1	3.4	4.1	2	24.4	16.4	15.9	15.8	16.3	25.1	21.2	19.7	17.2	14.3	17.4	23.4	24.5	21.6	17.4	2.7	4.5	4.2
Ti	1.203	1805	767	2618	516	2681	2151	2861	4371	1259	986	1509	264	4762	6239	5524	6025	6370	7209	6449	7877	6279	5289	5282	6639	6035	4251	5314	931	1940	1113
V	1.5	14	6	5	3	4	12	16	33	4	2	9	8	175	78	80	78	87	196	197	108	82	73	160	202	162	174	163	2	3	4
Cr	1	2	2	1	2	2	2	3	4	4	2	3	2	486	10	9	9	10	80	43	7	9	5	5	58	364	780	5	1	2	1
Mn	0.41	231	203	604	72	221	544	472	1118	931	458	101	130	1055	1232	1018	888	1211	1221	1082	1490	970	1427	911	1111	1197	1265	950	172	279	421
Ni	1	4	3	2	3	3	4	3	6	4	5	5	9	161	14	13	11	23	103	90	12	14	8	9	92	117	306	11	4	4	4
Cu	1	1	3	5	2	3	4	5	6	6	2	2	1	19	18	11	6	39	76	52	15	23	10	11	26	16	21	19	4	5	2
Zn	1	29	43	59	4	55	60	52	104	49	37	28	8	84	97	89	78	89	82	99	115	91	129	91	97	96	80	92	23	49	18
Ga	0.025	10.6	13.6	14.8	4.4	19.7	18	18.4	19.8	17.3	15.3	14.9	24.6	16.6	18.4	19.2	18.7	18	19.3	18.8	19.9	17.9	19	20.6	19.5	16.5	16	19.6	16.7	15.6	17
As	5	<5	10.4	<5	<5	<5	<5	<5	<5	<5	<5	<5	<5	<5	<5	<5	<5	<5	<5	<5	<5	<5	<5	<5	<5	<5	<5	<5	<5	<5	9.1
Rb	0.044	117.4	211	155.2	291.9	177.8	154.8	143.8	118.7	226.5	312.1	271.6	798.1	20.3	130.3	119.7	122.8	114.7	93.5	75.1	108.2	159.9	79.3	94.3	69.7	44	19.1	115.6	266.9	259.5	259.3
Sr	1	51	31	229	19	139	120	164	224	50	31	78	20	706	333	281	202	348	537	515	397	583	219	348	473	932	560	363	71	43	169
Y	0.005	33.7	29.2	37.4	17.5	35.2	29.2	32.4	45.2	26.2	60.4	44.1	101.9	22.8	37.9	40.4	37.7	45.5	24.3	25.8	45.4	37.3	34.2	27	26.3	24.7	18.4	26.8	35	38.9	45.3
Zr	0.035	299	139	460	95	321	329	393	355	293	231	233	147	148	420	402	442	412	165	163	282	437	208	216	165	169	132	209	162	472	194
Nb	1	19	22	18	17	18	15	19	18	14	22	20	43	6	15	15	15	15	8	9	17	15	19	11	9	9	6	11	16	22	32
Mo	0.023	0.14	0.54	1.12	0.34	1.48	0.93	4.42	0.76	0.66	1.11	0.46	0.24	0.3	0.75	0.62	0.61	0.96	0.77	0.56	1.13	0.3	0.84	1.41	0.47	0.53	0.22	0.72	0.82	1.33	16.38
Ag	0.01	0.03	0.05	1.07	0.03	0.09	0.07	0.14	0.06	0.1	0.04	0.05	0.05	0.05	0.11	0.13	0.06	0.15	0.05	0.08	0.12	0.09	0.05	0.08	0.07	0.07	0.06	0.09	0.08	0.15	1.52
Cd	0.024	<0.23	<0.23	<0.23	<0.23	<0.23	<0.23	<0.23	<0.23	<0.23	<0.23	<0.23	<0.23	0.1	<0.23	0.1	<0.23	<0.23	0.3	0.1	0.4	<0.23	0.2	0.1	0.1	0.2	0.1	0.1	<0.23	<0.23	<0.23
Sn	0.011	2.87	2.5	2.35	1.55	3.05	2.39	2.91	2.86	2.63	7.21	4.19	10.65	1.17	2.42	2.83	2.39	2.55	1.4	1.64	2.83	2.38	2.95	2.1	1.68	1.84	1.29	1.92	2.94	5.38	1.75
Sb	0.053	0.21	0.54	0.16	0.14	0.12	<0.06	0.14	0.21	<0.06	0.44	0.11	0.24	0.13	<0.06	0.07	0.56	0.23	0.23	0.28	0.09	0.07	0.13	<0.05	<0.05	0.35	0.06	0.07	0.21	0.22	0.1
Te	0.091	<0.37	<0.37	<0.37	<0.37	<0.37	<0.37	<0.37	<0.37	<0.37	<0.37	<0.37	<0.37	<0.09	<0.37	<0.09	<0.37	<0.37	<0.37	<0.09	<0.09	<0.37	<0.37	<0.09	<0.09	<0.09	<0.09	<0.09	<0.37	<0.37	<0.37
Cs	0.004	1.27	3.33	2.41	2.19	1.61	1.22	1.8	1.07	4.23	3.47	2.38	7.33	1.17	2.64	2.6	1.52	0.92	2.95	4.38	1.9	6.17	1.27	1.97	3.41	2.22	1.23	1.84	3.67	2.88	3.4
Ba	4	584	199	2691	193	1871	1353	1315	1925	1067	175	983	181	430	2390	2270	2362	6324	600	503	1587	2363	708	1045	502	1405	627	1050	568	266	456
La	2	41	41	68	17	73	54	67	96	66	113	86	35	28	58	59	62	69	24	24	44	59	32	44	24	42	24	41	60	57	84
Ce	0.012	131	71.5	127	38.1	136.5	104.1	139.3	145.6	131.8	202.5	164.7	81.1	56.3	116.7	120.9	120.8	123.7	52.9	50.2	95.3	120	67.3	85.6	52.7	93.3	51.9	82	98.7	150.4	163.5
Pr	0.002	10.99	8.05	15.48	3.82	16.53	12	16.16	19.55	14.59	23.62	17.63	10.18	7.05	14.64	14.54	15.15	16.91	6.7	6.31	12.23	14.91	8.87	9.71	6.61	11.58	6.43	9.42	11.87	12.54	18.46
Nd	0.009	43.3	27.7	60.3	12.6	62.4	44.1	59.6	72.7	51.5	80	58.8	36.9	28.5	58.8	56.5	60.7	68.6	27.7	26.2	51.1	59.1	37.5	35.9	27.1	47	25.9	35.1	41.7	43.6	67.5
Sm	0.007	8.85	4.76	10.53	2.54	11.07	7.6	10.13	11.78	8.21	13.7	9.89	10.2	5.51	10.83	10.64	11.05	12.36	5.78	5.59	10.32	10.98	7.61	6.43	5.76	8.73	5.02	6.4	7.12	7.69	12.37
Eu	0.002	1	0.52	2.25	0.23	2.49	1.17	1.86	2.28	1.14	0.33	0.87	0.05	1.5	2.97	2.93	3.02	3.34	1.58	1.54	2.78	2.98	1.85	1.56	1.55	2.15	1.32	1.53	0.85	0.62	0.87
Gd	0.006	7.04	4.2	8.53	2.59	8.95	6.45	7.58	9.87	6.33	10.96	8.09	11.11	4.76	9.28	9.1	9.17	10.69	5.31	5.17	9.26	9.32	6.87	5.46	5.36	6.7	4.16	5.41	6.37	6.81	10.05
Tb	0.001	1.08	0.76	1.25	0.46	1.33	0.99	1.12	1.43	0.93	1.73	1.33	2.42	0.72	1.38	1.36	1.36	1.58	0.83	0.83	1.4	1.36	1.05	0.84	0.83	0.91	0.62	0.85	1.03	1.17	1.53
Dy	0.004	6.12	4.85	6.93	2.7	7.12	5.59	6.03	8.22	5.13	10.14	7.8	16.41	4.17	7.49	7.62	7.48	8.68	4.74	4.8	8.04	7.52	6.05	4.82	4.86	4.78	3.5	4.9	6.08	6.98	8.26
Ho	0.001	1.23	1.02	1.35	0.54	1.32	1.09	1.16	1.63	0.98	2.05	1.56	3.52	0.83	1.43	1.51	1.43	1.63	0.91	0.96	1.62	1.42	1.22	0.98	0.97	0.92	0.69	0.98	1.21	1.42	1.57
Er	0.003	3.79	3.28	3.95	1.69	3.7	3.21	3.42	4.76	2.9	6.21	4.9	11.99	2.35	4.08	4.16	4.04	4.52	2.62	2.68	4.48	4.01	3.66	2.75	2.7	2.46	1.94	2.79	3.65	4.35	4.5
Tm	0.003	0.57	0.53	0.58	0.26	0.52	0.47	0.51	0.68	0.42	0.94	0.76	2.05	0.35	0.57	0.61	0.58	0.62	0.37	0.39	0.67	0.56	0.56	0.41	0.41	0.35	0.28	0.41	0.55	0.65	0.66
Yb	0.003	3.66	3.58	3.66	1.77	3.29	3.07	3.22	4.23	2.63	5.97	5.05	14.09	2.14	3.63	3.75	3.55	3.75	2.34	2.41	4.15	3.44	3.69	2.55	2.42	2.12	1.73	2.55	3.46	4.26	4.09
Lu	0.003	0.57	0.56	0.57	0.28	0.51	0.46	0.5	0.65	0.4	0.91	0.78	2.12	0.32	0.56	0.55	0.53	0.57	0.36	0.36	0.62	0.53	0.57	0.37	0.36	0.31	0.26	0.38	0.53	0.67	0.62
Hf	0.004	8.4	5.59	11.11	3.88	8.75	8.45	9.86	9.27	7.87	8.21	7.59	9.95	3.51	10.28	9.61	10.54	9.9	4.32	4.19	7.23	10.45	6.47	5.44	4.24	4.22	3.35	5.36	5.54	12.83	6.77
Ta	0.002	1.51	1.28	1	1.75	1.62	1.29	1.38	1.24	1.29	2.5	2.35	7.93	0.51	1	0.9	0.8	0.81	0.55	0.67	0.99	0.73	1.33	0.86	0.61	0.63	0.52	0.74	2.26	2.05	2.84
Tl	0.01	0.64	1.01	0.75	1.6	0.95	0.81	0.76	0.68	1.12	1.43	1.25	2.87	0.1	0.58	0.59	0.64	0.57	0.29	0.29	0.55	0.93	0.37	0.63	0.25	0.23	0.1	0.72	1.4	1.31	1.31
Pb	1.5	10	11	4	6	34	31	37	16	42	7	8	40	10	24	18	14	11	8	19	25	26	6	30	9	14	10	49	37	42	21
Bi	0.01	0.16	0.01	0.03	0.07	0.17	0.04	0.23	0.07	0.12	0.06	0.09	0.06	0.25	0.08	0.07	0.12	0.11	0.02	0.1	0.11	0.15	0.15	0.05	0.02	0.17	0.07	0.04	0.67	0.23	0.01
Th	0.002	17.8	21.8	12.3	16.4	18.7	11.8	19.5	18.2	19.3	47.1	45.7	48.7	3.9	9.7	11.3	8.9	8.2	4.1	4.4	11.7	10	13.4	10.1	4.4	7.8	4.4	10	27.1	33.7	40.9
U	0.002	2.69	1.31	0.99	1.38	0.76	2.21	4.59	3.79	3.84	9.17	2.47	8.25	0.6	1.91	1.81	2.74	0.6	0.64	5.25	4.88	1.89	2.77	2.15		1.62	1.52	8.11	1.75	0.6	0.93
tot Alk		7.53	6.94	9.62	8.63	9.6	8.67	9.24	7.82	8.51	8.58	8.66	8.72	3.28	8.66	8.66	8.57	8.45	6.14	5.58	6.85	7.79	7.23	7.11	3.17	3.17	3.71	7.23	8.79	8.76	9.36
MALI		7.42	6.77	8.84	8.32	9.05	7.85	8.3	6.97	8.05	7.89	8.52	8.31	-5.8	5.9	5.79	7.56	7.35	-1.4	-2.23	2.36	6.36	5.79	3.07	-5.99	-6.08	-3.99	3.27	8.19	8.48	8.82
ASI		1.11	1.49	1.17	0.98	1.07	1.05	1.1	1.25	1.14	1.06	1.1	1.06	1.22	1.04	1.05	1.2	1.21	1.11	1.13	1.07	1.33	1.19	1.04	1.21	1.19	1.15	1.06	1.04	1.04	1.05
FeOt/(FeOt+MgO)		0.68	0.69	0.6	0.32	0.93	0.86	0.73	0.75	0.89	0.76	0.84	0.82	0.78	0.83	0.87	0.54	0.71	0.77	0.64	0.62	0.63	0.64	0.74	0.68	0.61	0.76	0.54	0.54	0.52	0.75
K2O/Na2O		1.15	5.45	1.46	7.06	1.49	1.36	1.11	0.78	3.53	2.34	1.92	1.19	0.22	1.17	1.13	1.21	1.48	0.73	0.43	1.01	1.56	0.48	0.8	0.2	0.19	0.18	0.96	2	2.33	1.89
La/Yb		11.17	11.35	18.63	9.68	22.06	17.72	20.87	22.75	24.92	18.89	17.05	2.45	13	16.03	15.77	17.57	18.45	10.33	10.01	10.53	16.99	8.66	17.41	9.7	19.84	13.66	15.92	17.28	13.39	20.61
Zr/Hf		35.66	24.81	41.43	24.5	36.71	38.92	39.86	38.31	37.19	28.15	30.64	14.79	42.24	40.88	41.88	41.95	41.67	38.3	38.94	38.95	41.83	32.19	39.7	39	39.97	39.3	39.03	29.18	36.77	28.65
Th/U		6.63	16.65	12.38	11.88	24.72	5.32	4.25	4.8	5.04	5.13	18.48	5.91	6.55	5.06	6.26	3.26	13.63	6.42	0.85	2.4	5.32	4.85	4.68		4.82	2.91	1.24	15.45	55.84	43.81
M		1.23	0.93	1.39	1.37	1.45	1.46	1.46	1.33	1.27	1.39	1.28	1.36	2.67	1.89	1.89	1.44	1.47	2.68	2.66	2.1	1.39	1.5	2.05	2.72	2.77	2.68	2.01	1.39	1.35	1.41
Zrn satur T(°C)		858	809	888	745	846	848	865	866	852	820	829	782	-	-	-	-	-	-	-	-	-	-	-	-	-	-	-	787	894	802

Major elements by XRF, trace elements by ICP-MS, except V, Cr, Ni, Cu, Zn, Sr, Nb, Ba, and Pb by XRF

(MI) samples from which melt inclusions were analysed, * from Agangi et al. (2010), ** from Agangi et al., 2011. M = (Na+K+2Ca)/(Si?Al) and zircon saturation temperature (Watson and Harrison, 1983)

A andesite, B Basalt, BD Bunburn Dacite, CD Chandabooka Dacite, ChD Childera Dacite, GHVC Glyde Hill Volcanic Complex, CVC Chandabooka Volcanic Complex, FE felsic enclave (granite inclusion), HS Hiltaba Suite granite, LGR Lake Gairdner Rhyolite, MDS Moonamby Dyke Suite, RD Rhyolite-dacite, WP Waurea Pyroclastics, WR Wheepool Rhyolite, YRD Yantea Rhyolite-da

Table 5. Selected melt inclusion analyses

Melt inclusion		19C 33-12	3D 33-75	17D 32-59	05D 33-39	02D 33-23	06D 33-72	5u 10-19	19u 19-46	15 31-39	21d	23d 19-12	18D 42-47	2C b 36-5C	2C a 36-5C	6C c 35-24	6C a 35-24	3 21-60	13C a 35-6	27D 28-38	21C a 14c-	10C b 35-4	10C a 35-4	10C c 35-4	19 17-20	26d 28-33	14d 28-2
		1	2	3	4	5	6	7	8	9	10	11	12	13	14	15	16	17	18	19	20	21	22	23	24	25	26
		heated	heated	heated	heated	heated	heated	heated	heated	heated	unheated	unheated	unheated	heated	heated	heated	heated	unheated	heated	unheated	heated	heated	heated	heated	heated	unheated	unheated
Sample		GH15	GH15	GH15	GH15	GH15	GH15	GH13	GH13	GH95	GH95	GH95	GH95	GH23	GH23	GH59	GH59	GH06	GH59	GH59	GH06	GH59	GH59	GH59	GH23	GH59	GH59
Unit	detection li	MDS	MDS	MDS	MDS	MDS	MDS	WP	WP	WP	WP	WP	WP	WR	WR	WR	WR	WR	WR	WR	WR	WR	WR	WR	WR	WR	WR
SiO2 (wt.%)		76.56	76.82	76.01	76.33	77.05	76.43	82.66	80.18	78.12	72.7	72.66	72.61	77.12	72.43	79.2	78.87	74.08	71.52	70.9	72.85	73.8	73.52	71.95	71.42	72.33	71.3
TiO2		0.22	0.17	0.17	0.11	0.12	0.1	<dl	0.13	0.1	<dl	0.16	0.16	0.21	0.2	0.15	0.15	0.27	0.16	0.07	0.26	0.2	0.1	0.08	<dl	0.12	<dl
Al2O3		11.57	11.91	12.77	11.41	11.87	11.81	9.24	10.14	12.63	15.86	16.02	16.13	11.43	14.71	10.04	10.4	15.07	14.71	16.4	15.13	13.71	13.97	14.89	15.35	15.49	16.36
Fe2O3		1.34	1.25	1.26	1.35	1.31	1.38	0.58	0.52	0.62	0.25	0.41	0.52	1.05	1.21	0.91	0.87	0.95	1.17	0.39	0.84	0.98	1.12	0.64	1.14	0.58	0.22
MgO		<dl	<dl	0.02	0.03	0.02	0.04	<dl	0.05	0.05	<dl	<dl	<dl	0.09	0.15	0.09	0.09	0.11	0.15	<dl	0.1	0.09	0.08	0.13	0.12	<dl	<dl
CaO		0.58	0.54	0.61	0.51	0.51	0.53	0.29	0.41	0.42	0.15	0.37	0.3	0.4	0.64	0.33	0.34	0.51	0.7	0.22	0.39	0.56	0.47	0.69	0.54	0.46	0.38
Na2O		4.7	4.05	3.58	5.23	4.05	4.11	2.35	4.43	3.28	4.45	4.03	4.31	4.49	3.51	3.92	3.67	2.27	3.88	3.78	6.21	3.53	3.44	3.8	2.9	3.82	3.45
K2O		4.69	4.83	5.07	4.53	4.59	5.16	4.82	4.03	4.46	6.19	5.89	5.7	4.59	5.87	4.93	5.17	6.47	6.34	6.97	4.18	6.34	6.6	7.02	7.16	6.34	7.15
Cl		0.08	0.12	0.14	0.14	0.17	0.13	0.05	0.11	0.07	0.11	0.11	0.09	0.05	0.09	0.05	0.06	0.13	0.1	0.13	0.04	0.06	0.06	0.08	0.08	0.08	0.06
F		0.26	0.31	0.36	0.36	0.31	0.31	0	<dl	0.25	0.29	0.34	0.17	0.58	1.19	0.38	0.38	0.14	1.28	1.13	0	0.71	0.63	0.7	1.3	0.78	1.07
total		100	100	100	100	100	100	100	100	100	100	100	100	100	100	100	100	100	100	100	100	100	100	100	100	100	100
H2O*		2.48	3.08	3.98	2.53	2.27	3.5	1.46	0.64	0.16	1.26	3.55	1.05	3.62	1.31	1.15	1.42	4.58	0.32	0.83	-	0.35	1.74	1.69	0.66	0.03	1.68
Li (ppm)	3.73	17.94	11.04	12.14				28.14					<5.23	13.61	6.65	11.9	13.89	53.55	8.34	9.33	32.94	9.67	12.72	13.32	2.56		
Be	5.18	<10.11	4.85	7.2				<4.72					<6.47	4.94	<5.05	<4.40	<10.84	<16.03	5.39	<15.70	<4.53	3.24	4.49	5.61	<2.51		
B	66.04	<108.83	<43.85	26.55				<46.71					<98.27	<54.23	<66.29	<49.44	<90.56	<249.62	<52.83	<214.18	<38.66	<25.10	<9.73	21.24	<13.92		
Al	171.7	63507.26	63507.26	68799.53				47630.44					84676.34	58214.99	79384.07	52922.71	52922.71	79384.07	79384.07	84676.34	79384.07	74091.8	74091.8	79384.07	79384.07		
P	108.61	<218.79	<66.15	56.59				<66.67					<177.64	<67.77	<119.54	<81.90	<207.17	<357.08	<106.76	<303.17	77.31	<33.82	40.94	48.06	<25.77		
Ca	1979.96	<3427.02	4013.52	4151.29				1997.92					<3675.99	3168.41	5609.85	<1548.24	<3575.65	<5867.81	4548.89	<6447.26	3942.17	4088.22	3551.47	3904.55	4018.85		
Ga	0.65	15.42	15.35	19.35				12.74					17.163	13.93	15.78	13.33	13.06	17.03	17.01	21.96	17.14	12.98	14.55	15.03	16.1		
Rb	1.35	336.73	370.55	394.24				253.47					354.347	237.17	293.8	233.26	231.17	338.13	294.61	377.31	203.54	287.99	290.9	311.5	313.02		
Sr	0.21	19.44	8.45	7.12				0.37					<0.35	15.01	21.6	9.23	5.4	0.83	34.02	8.35	18.7	12.35	10.79	14.2	16.8		
Zr	0.44	200.03	191.81	235.25				93.79					145.817	136.07	234.66	102.85	111.74	162.12	170.66	128.19	224.99	104.95	109.15	109.73	218.53		
Nb	0.27	21.8	26.23	24.94				22.03					31	20.6	30.52	21.69	22.82	33.92	25.75	35.63	31.17	24.96	25.21	20.96	27.05		
Sn	5.56	<10.82	9.03	10.13				4.26					<9.69	5.84	7.6	<3.58	<9.92	<21.70	7.341	<14.65	5.79	4.22	4.22	4	5.09		
Cu	6.34	121.37	32.39	10.19				1154.14					<8.67	53.53	11.13	167.09	217.79	1818.08	32.9	<22.30	128.28	75.24	82.62	89.93	55.28		
Zn	3.91	45.41	44.17	40.56				64.28					42.58	46.4	60.3	42.9	51.68	100.52	64.65	25.37	52.72	45.72	46.06	52.8	67.43		
Cs	0.44	8.39	9.67	10.85				5.82					10.227	6.14	6.58	7.47	7.61	8.39	6.26	27.97	3.67	8.96	9.27	9.64	7.65		
Ba	1.27	142.05	28.66	14.12				<1.33					1.881	114.12	183.53	48.11	14.38	<10.70	252.26	2.86	90.56	87.39	66.36	111.41	127.95		
La	0.12	79.5	89.88	91.22				22.7					12.424	47.17	76.6	28.61	27.99	41.74	72.14	41.76	69.53	39.14	37.09	38.28	59.86		
Ce	0.12	168.97	205.18	199.01				52.2					19.872	113.51	175.68	74.79	73.39	89.03	160.1	72	155.01	86.01	81.41	80.18	142.81		
Pr	0.11	15.73	18.08	19.82				4.35					1.712	11.71	17.09	7.01	7.15	8.84	17.48	5.71	15.81	8.54	8.09	7.75	13.63		
Nd	0.64	67.29	64.6	65.77				13.85					4.64	46.01	65.52	27.24	28.94	29.93	61.2	11.18	53.67	27.82	26.14	24.95	46.64		
Sm	0.67	7.95	10.43	12.55				2.43					1.298	8.61	12.52	4.83	7.38	4.23	9.52	2.24	10.25	5.48	5.39	5.15	8.12		
Eu	0.17	0.6	0.31	0.25				<0.10					<0.25	0.41	1	0.42	0.52	0.62	0.71	<0.36	0.76	0.41	0.41	0.5	0.79		
Gd	0.53	10.18	9.74	10.57				1.71					0.864	5.92	10.94	4.71	5.63	7.44	8.64	1.59	8.98	4.67	3.85	3.73	6.06		
Tb	0.08	1.16	1.43	1.71				0.46					0.291	0.97	1.63	0.81	1.04	0.73	1.72	<0.30	1.43	0.63	0.66	0.51	0.99		
Dy	0.35	6.93	9.66	10.7				2.17					2.202	7.16	8.7	4.8	5.87	4.49	8.7	1.01	9.35	5.18	4.63	3.59	6.79		
Ho	0.07	1.77	1.78	2.02				0.49					0.442	1.27	1.82	1.01	0.95	1.01	1.75	0.24	1.82	0.98	1.04	0.68	1.26		
Y	0.18	43.93	51.87	61.19				18.03					18.21	35.98	54.11	30.23	32.85	33.58	50.14	13.25	51.12	28.67	27.99	23.2	38.69		
Er	0.26	4.43	5.93	6.75				1.74					2.553	3.65	6	3.37	3.03	3.1	5.81	1.25	5.68	3.34	2.96	2.19	4.06		
Tm	0.09	0.85	0.86	0.97				0.35					0.335	0.58	1.07	0.49	0.49	0.58	0.9	<0.32	0.79	0.44	0.49	0.36	0.64		
Yb	0.34	3.63	6.52	6.37				2.54					2.96	3.91	5.21	2.93	3.43	3.65	5.77	2.31	6.48	3.56	3.8	2.55	4.32		
Lu	0.08	0.74	0.74	1.08				0.25					0.324	0.56	1.02	0.49	0.57	0.66	0.82	0.34	0.74	0.61	0.56	0.43	0.58		
Hf	0.27	6.05	6.76	8.7				4.31					5.971	5.39	8.59	4.04	4.39	6.05	6.14	5.31	8.19	4.33	4.4	4.5	6.99		
Ta	0.08	1.36	1.79	2.13				1.29					1.942	1.28	2.06	1.43	1.22	1.67	1.78	2.47	2.29	1.71	1.62	1.62	1.59		
Ti	11.76	1333.04	1100.52	1056.54				637.97					843.08	1548.15	2118.99	1078.95	1179.75	1137.24	1426.35	564.32	2133.24	1060.85	1169.88	595.88	1294.94		
Pb	0.85	41.63	48.6	48.07				37.61					43.691	33.66	43.25	30.78	31.08	50.8	39.56	54.52	68.12	37.31	39.67	43.97	45.52		
Th	0.1	36.56	46.45	46.12				18.47					19.679	17.92	29.01	20.31	20.35	27.35	27.3	50.21	38.43	28.44	27.53	26.84	25.17		
U	0.09	8.76	11.12	11.07				4.61					6.044	4.45	6.32	5.56	6.65	6.37	6.14	14.31	7.15	6.95	6.68	7.49	6.88		
tot Alk		9.4	8.89	8.65	9.76	8.64	9.26	7.17	8.46	7.75	10.65	9.92	10.01	9.08	9.38	8.85	8.83	8.74	10.22	10.76	10.39	9.86	10.04	10.83	10.06	10.15	10.59
MALI		8.81	8.34	8.04	9.25	8.13	8.73	6.88	8.05	7.33	10.5	9.54	9.71	8.68	8.74	8.52	8.49	8.23	9.52	10.54	10	9.3	9.57	10.13	9.51	9.69	10.22
ASI		0.87	0.96	1.07	0.82	0.98	0.92	0.99	1.18		1.12	1.2	1.19	0.9	1.16	0.83	0.87	1.35	1.06	1.17	1	1.04	1.06	1.03	1.18	1.14	1.19
FeOt/(FeOt+MgO)		-	-	0.98	0.98	0.98	0.97	-	0.91	0.92	-	-	-	0.91	0.88	0.9	0.9	0.89	0.87	-	0.88	0.9	0.93	0.82	0.9	-	-
K2O/Na2O		1	1.19	1.42	0.87	1.13	1.26	2.05	0.91	1.36	1.39	1.46	1.32	1.02	1.67	1.26	1.41	2.84	1.63	1.84	0.67	1.8	1.92	1.85	2.47	1.66	2.07
La/Yb		21.92	13.78	14.32				8.93					4.197	12.06	14.72	9.76	8.17	11.45	12.5	18.06	10.72	11	9.75	15.03	13.86		
Zr/Hf		33.04	28.35	27.05				21.77					24.42	25.24	27.32	25.47	25.43	26.79	27.8	24.14	27.46	24.23	24.79	24.4	31.27		
Th/U		4.17	4.18	4.17				4					3.26	4.02	4.59	3.65	3.06	4.29	4.45	3.51	5.38	4.09	4.12	3.58	3.66		
M		1.57	1.41	1.3	1.65	1.38	1.47	1.25	1.52	1.11	1.16	1.13	1.12	1.47	1.27	1.54	1.48	1.03	1.41	1.16	1.34	1.35	1.31	1.41	1.23		
Zrn satur T(°C)		793	801	829				752					799	767	831	739	750	815	791	784	821	754	760	753	827		

Major element oxides by EPMA recalculated to 100% anhydrous, trace elements by LA-ICP-MS

WR Wheepool Rhyolite, WP Waurea Pyroclastics, MDS Moonamby Dyke Suite. M = (Na+K+2Ca)/(Si?Al), and Zircon saturation temperature (Watson and Harrison, 1983)

* H2O by difference 100 - EPMA total